

Miscellaneous Calculations for a Fully Electrostatic Proton EDM Experiment, Version II

(Extension of Version I, with obsolete sections eliminated,
and incorporating results due to other pEDM'ers),

Richard Talman

May 3, 2010

Abstract

The main bending field for the proposed proton EDM experiment has to be electrostatic. Though the necessary focusing could be produced magnetically, this would cause the optics to be different for the counter-rotating proton beams. Here we limit discussion to electrostatic focusing, with no magnets whatsoever in the ring.

A few electrostatic cells and lattices of both combined and separated function type have been considered in an earlier version of this note. A combined function CDSF-AG lattice and a separated function lattice SF-AG were analysed and shown to be practical. But this material has been deleted from the present report because subsequent studies have shown that only weaker (and hence easier) focusing is desirable. Simple curved-planar electrodes are now assumed because the strong focusing made possible by toroidally-shaped electrodes is not needed.

The ameliorating effect of synchrotron oscillations on spin depolarization is studied. Spin motion of a beam with finite momentum spread but vanishing betatron amplitudes is described, and a compensation scheme minimizing spin decoherence is derived. A scheme (using sextupoles) for compensating decoherence due to betatron oscillations, is then described, bringing to three the number of constraints to be imposed on the lattice.

A weak FODO lattice satisfying the three decoherence constraints is described. Though decoherence-compensated, this lattice has to be rejected because it “sits on transition”. To avoid transition the horizontal tune is therefore increased, yielding a “less weak”, fully-compensated, separated function lattice. It includes long straight sections, but none of the RF, injection, polarimetry equipment for which the long straights are essential.

Contents

1	Outline of Report, Possible Configurations, and Disclaimers	4
2	Separated Function Electrostatic Lattices	7
2.1	Electrostatic Quadrupoles Focal Lengths	7
2.2	Horizontal Focusing Transfer Matrices	9
2.3	Achievable Electrostatic Quadrupole Focusing Strength	10
3	Unequal Tune FODO Lattice Design	11
3.1	Longitudinal Variation of the Lattice Functions	14
3.2	Setting the Tunes	15
3.3	Compensation For Dipole Focusing	16
3.4	Beam Acceptance and Cell Length Determination	16
4	Combined Function Electrostatic Bending Elements	18
4.1	Field Calculation	18
4.2	Chromatic Deflection	21
5	Thin Element Representation of Electrostatic Bend/Lens	22
6	Electric Parameterization Via Conventional Magnet Formalism	24
6.1	Matching to Conventional Formalism	24
6.2	Transfer Map Determination	26
7	Space Charge Issues	27
7.1	Introduction	27
7.2	Beam-Beam Tune Shift	27
7.3	Space Charge (Laslett) Tune Shift	28
7.4	Luminosity	30
7.5	p-p Collision Rates	31
8	Synchrotron Oscillations and Spin Precession	32
8.1	Averaging Over Energy	32
8.2	Spin Precession	37
8.2.1	Small Amplitudes, No Deviation from “Magic” Condition	37
8.2.2	Deviant Beam Energy	41
9	Betatron-Induced Decoherence	41
10	Curved-Planar (Weak) Separated Function FODO Lattice	44
11	Qualitative Discussion of Betatron-Induced Decoherence	49
12	Betatron Decoherence Compensation	50
13	Curved-Planar (Less Weak) Separated Function FODO Lattice and Incorporation of Long Straight Sections	56

14 Numerical Examples	60
A APPENDICES	63
A.1 Excess Path Length Resulting from Betatron Oscillation	63
A.1.1 Horizontal Betatron Oscillations	63
A.1.2 Vertical Betatron Oscillations	64
A.2 Relation Between Dispersion Function and the Closed Orbit Path Length Deviation Caused by a Local Deflection	65
A.3 Sextupole Chromatic Neutrality	66

Acknowledgement

This report started out with the limited goal of designing and describing fully electrostatic lattice options for the proton EDM experiment. It has evolved into a broader review of experimental methods for the experiment. Most of these were well understood before I was even aware such an experiment was being contemplated. Unaware of the chronology, rather than attempting to figure out the origins of the various ideas, I simply lift results from various reports (especially from the December, 2009, BNL review) and from numerous conversations, without accompanying attribution; even including gratuitous pedagogical derivations of well known results in some cases. The title page parenthetical phrase “(incorporating results due to other pEDM’ers)” is intended to convey this. Only a few of the ideas are original, and *they* may not be “good” ideas. One is the proposal to use beam-beam collisions to monitor the beam polarization. Though intriguing and instructive I have now shelved this idea and deleted it from the report. This led naturally to the possibility of stabilizing the beam polarization by feeding back from the up-down scattering asymmetry to the RF frequency.¹ The discussion of compensation against spin decoherence using sextupoles, while worked out from scratch, is probably equivalent to previous discussions by Yuri Orlov.

1 Outline of Report, Possible Configurations, and Disclaimers

As its title indicates, this report contains miscellaneous calculations relating to the implementation of a fully electrostatic proton EDM storage ring. The contents can best be inferred from the table of contents. The sections listed there are largely independent and their order largely arbitrary. Discussions within sections are intended to be elementary and self-contained. That is, (almost) everything is calculated from scratch, with handbook formulas introduced eventually only for corroboration and extension. Though this may make the paper hard to read, it is supposed to make it easy to understand, criticize, modify, extend, and so on.

Various lattice designs have been investigated with various features emphasized. Some were described in a preliminary version of this report. It has been practical to distill many features into a single lattice which is described in detail in this version.

Two lattice options, both strong alternating gradient rings, seemed initially to be the most promising for the proton EDM experiment. Simplicity and other considerations favored a separated function, FODO, alternating gradient (SF-AG) option for focusing in both planes. But, to obtain very

¹Bill Morse explains that this would work as follows. By modulating ω_{RF} about its currently best value, the angle α of the polarization vector is intentionally swept left and right. The up-down asymmetry observed in scatters is proportional to α . If the up-down asymmetry is larger for α modulated to the left than for α modulated to the right, it shows that the central value of α is biased to the left and needs to be moved to the right.

unequal horizontal and vertical tunes, which were considered likely to be desirable, a hybrid, combined-defocusing, separated-focusing (CDSF-AG) lattice was also studied. For ideal combined-function vertical focusing the electrodes would be toroidal but, for design convenience, the electrodes were taken to be (azimuthally-limited) circular cylinders. With this 2D idealization, the electric field can be calculated exactly using conformal mapping. A circular orbit of radius r_0 is obtained by setting the major toroidal radius to that value and the minor toroidal axis to provide the appropriate focusing strength. It seemed simpler to provide the opposite sign, horizontal focusing by lumped quadrupoles rather than by combined function, saddle-shaped toroidal electrodes. As mentioned already, because only quite weak focusing will be required, much of this material is now obsolete. But, this material has been retained in the report as it contains discussion of the treatment of electrostatic (as contrasted with magnetic) elements.

Slow extraction onto the carbon polarimeter was considered in some detail for the CDSF-AG case in the earlier version of the report. That material, highly specific to the CDSF-AG lattice, has been deleted and will have to be reproduced for lattices that now seems more practical. Also deleted from this report is the design of lattices synchronized to the bunch pattern. This design was predicated on p-p polarimetry and/or current balancing using resonant beam current monitors. Since both of these ideas now seem obsolete this material has also been deleted.

For calculating particle orbits and lattice functions it is convenient to exploit existing accelerator codes, such as MAD and UAL, that assume magnetic bending and focusing. To accomplish this one can introduce effective bend angle $\Delta\theta_{\text{eff}}^{(E)}$, effective quadupole coefficient $K_{1,\text{eff}}^{(E)}$, and so on. All studies in this report are based on this form of treatment. For more refined future optimization and simulation it will be appropriate to incorporate electric field effects into the descriptions in a more transparent way.

Section 7 describes space charge limitations. (Like the previous sections) much of this material was distributed previously to a few collaborators. After having repaired a few errors and misunderstandings pointed out by Alexei Fedotov, these formulas are in quite good agreement with his.

Section 8 analyses synchrotron oscillations and their effect on polarization preservation. Subsection 8.1 contains a derivation of standard synchrotron oscillation theory; by its use of difference rather than differential equations, the presentation is somewhat unconventional. The importance, for improved averaging and increased spin coherence time, of linearizing the dependence of relativistic γ -factor of revolution period $T(\gamma)$ is emphasized. Subsection 8.2 analyses spin precession (due to deviation from the magic energy) in the presence of synchrotron oscillations. Current lore seems to accept, because the equilibrium state of the proton axis is unstable, that inexorable monotonic deviation from the equilibrium orientation must occur. To the contrary the analysis in this section seems to imply that, other than slow drift (subject to correction by RF feedback) synchrotron amplitude, by itself, do not necessarily cause spin

decoherence.

The longitudinal focusing has to be at least strong enough to keep the wandering of the proton axis within reasonable bounds (certainly much less than $\pi/2$). Beyond that, further increase of RF voltage may be counter-productive because of the possibility of resonant-depolarization.

Spin decoherence caused by betatron oscillations is a serious problem. This is discussed in Section 9. Compensation against spin decoherence is discussed in Section 12. Eq. (164) is the fundamental formula determining the strengths S^A , S^B , and S^C of three sextupole families.

Accelerator formulas needed to obtain the compensation formulas are derived in three appendices.

To reduce betatron-induced spin decoherence both horizontal and vertical tunes have been reduced to quite small values. But not *too small* values, because a certain amount of lattice function variation is required to provide distinguishable locations for the required three sextupole families. Contrary to earlier expectations, however, it is found that enough variability can be designed into individual cells to avoid the need for lattice sectors dedicated to decoherence compensation.

The compensation formulas are applied in full numerical detail for an almost up-to-date lattice in Section 10. While analysing this lattice it was realized that the lattice was sitting almost exactly “on transition” which would surely be unacceptable. This called for increasing the horizontal tune.

My most up-to-date electrostatic lattice design is exhibited in Section 13. This lattice supercedes the lattice of Section 10 in two ways. Though the cell geometries are identical, the horizontal phase advance per cell, instead of being equal to the vertical phase advance, is three times greater. With the full lattice being circular, and consisting of nothing but repetitions of the basic cell, the same Eq. (164) is used to determine the sextupole strengths for this lattice.

The second major development described in Section 13 is the inclusion of long straight sections. These will be needed for for injection, RF, extraction, polarimetry and so on. None of these details have, as yet, been incorporated. Even with this simplification it turns out to be hard to incorporate straight sections without mangling the previously the already-achieved decoherence compensation.

It would be desirable for the dispersion to be zero in the long straights, but I found it impossible to achieve that without using bends large compared to the regular arc bends. I therefore backed off from this requirement and only matched the straight section optics to the previously-compensated arc optics. All this is exhibited in Section 13

Finally, some disclaimers: Consistent with the somewhat futuristic present stage of the project, quite a bit of wishful thinking has gone into the various lattice designs. Quad strengths have been taken at the high end of what is thought to be achievable, though a certain amount of freedom has been left to allow them to be longer but weaker. Active elements, bending elements, quadrupoles, and sextupoles take up all the longitudinal space, leaving no room for drift regions that will certainly be necessary for BPM's and other monitoring

devices. Remedying this may increase the circumference somewhat, but should not greatly affect the designs otherwise.

A more serious over-simplification that has been made, in the case of the SF-AG lattice synchronized to the bunch pattern, is that insufficient horizontal aperture has been provided in the high β_x regions of the arcs adjacent to low β IP's. Such a region is illustrated by the solid curves in Fig. ?? and subsequent figures. One can avoid this problem by replacing all the high- β_x IP's by high- β_y IP's (shown as broken lines in the various figures). This would take advantage of the generous vertical aperture in the electrostatic steering elements. And it would leave colliding beam issues unaffected. It would, however, wreck the scheme (thought to be needed for spin decoherence compensation) of having regions of vastly different beta functions at points of high dispersion. If the (as yet unconfirmed) claims concerning spin precession in Section 8 are valid, then the need for lattice spin compensation using sextupoles will be relaxed and high- β_x regions may be unnecessary.

Long straight sections have been made available for injection, extraction, RF and so on, but no attempt has been made to design these features. It is typical to have dispersion suppression at the ends of major arcs, but this has not been attempted here.

In agreement with Fedotov's calculations, the beam intensity required for measuring beam polarization using external carbon polarimetry seems fairly conservative. To make elastic p-p scattering polarimetry practical requires significantly more aggressive beam intensity assumptions. Other subtleties, such as hourglass effect, have been ignored. Also the above-mentioned wishful thinking about achievable element strengths is nowhere more applicable than to the design of the low-beta interaction point optics.

Intensity limitation due to intrabeam scattering (IBS) is not addressed. More to the point, the whole issue of the influence of IBS on the experiment deserves serious treatment of the sort that can perhaps be best provided by simulation. It has been understood that simulation is likely to play a significant role in calculating spin decoherence. But the analytic theory of decoherence due to lattice optics seems (to me) relatively straightforward compared to understanding the influence of intrabeam scattering.

2 Separated Function Electrostatic Lattices

2.1 Electrostatic Quadrupoles Focal Lengths

For a separated function electric FODO lattice one requires electrostatic quadrupoles. Fig. 1 indicates the design of the quadrupoles used in the muon g-2 experiment[2]. Since it will be important to achieve the highest possible gradient, it will probably be appropriate to shape the poles as in Fig. 2. This will reduce unwanted, non-quadrupole multipole content but, more important, it will increase the maximum achievable gradient. With the potential at the origin being zero, the electric potential on the y -axis will be $\phi = \text{constant } y^2$. This determines the

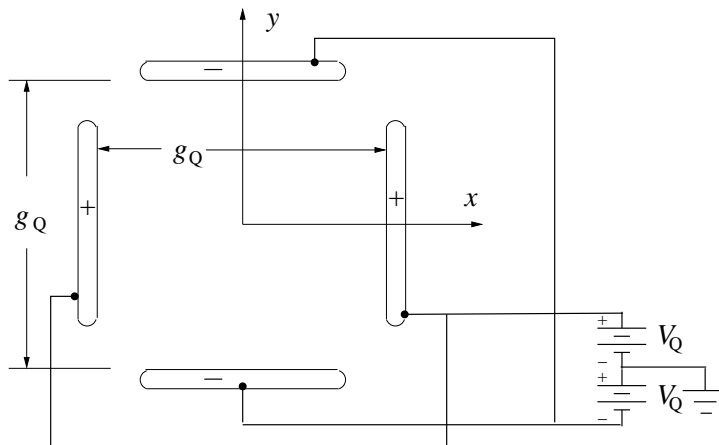


Figure 1: Schematic view of the electrodes of an electrostatic quadrupole with planar electrodes. For the AGS g-2 experiment, the gap length g_Q was 10 cm.

constant, in terms of voltage V_Q and gap g_Q to be $-V_Q/(g_Q/2)^2$. Then the electric fields are

$$E_y(x=0) = \frac{8V_Q}{g_Q^2} y, \quad \text{and} \quad E_x(y=0) = -\frac{8V_Q}{g_Q^2} x. \quad (1)$$

As drawn, this quadrupole is *focusing* in the x -plane. For protons of momentum p , and velocity v , let its focal length be f_x . In paraxial approximation, the deflection angle for displacement x is then

$$-\frac{x}{f_x} = \frac{\Delta p_x}{p} = \frac{1}{p} \frac{dp}{dt} \frac{l_Q}{v} = \frac{1}{p} e E_x \frac{l_Q}{v} = -\frac{1}{pc/e} \frac{8V_Q}{g_Q^2} x \frac{l_Q}{v/c} \quad (2)$$

where l_Q is the length of the element. The quadrupole coefficient K_1 (which is the inverse horizontal focal length per unit element length) is therefore

$$K_1 = \frac{1}{f_x l_Q} = \frac{V_Q}{\beta pc/e} \frac{8}{g_Q^2}. \quad (3)$$

(For the pEDM experiment, $\beta \approx 0.6$, and $pc/e \approx 0.7GV$, and a tentative value for g is 0.02 m.) The linearized equations of horizontal motion in the quadrupole are

$$\frac{d^2 x}{dz^2} = -K_1 x, \quad \text{and} \quad \frac{d^2 y}{dz^2} = K_1 y. \quad (4)$$

Regrettably the notation here is not universal. The signs have been chosen to conform to the MAD lattice description conventions. Positive K_1 indicates that the bending field strength increases with increasing x , which results in horizontal focusing. These same formulas will be applied to focusing in gently curving sector elements, but then extra “geometric” focusing terms have to be applied to account for the fact that x and y , rather than being purely Cartesian variables, are coordinates in a gradually rotating frame.

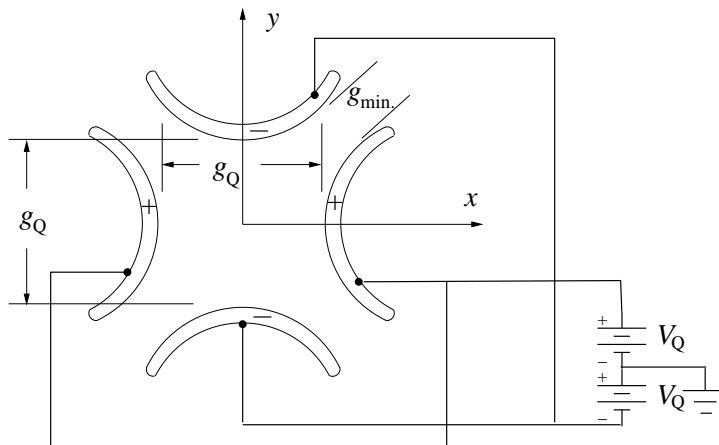


Figure 2: Schematic view of an electrostatic quadrupole with parabolic-shaped electrodes. For the proton EDM experiment $g_Q \approx 2$ cm (to match the gap width g in the bending elements) With appropriate filtering the electrodes can also serve as a beam position monitor (BPM). For simplicity this is assumed to be the case in this note.

2.2 Horizontal Focusing Transfer Matrices

It is assumed in all cases that horizontal focusing will occur primarily in electrostatic, separated function quadrupoles, (indicated by superscript “sf”) designed along the lines indicated in Section 2.1. Following Wollnik[8], (though not in detail) it is convenient to introduce positive real quantities k_x^{sf} and k_y^{sf} in terms of which the equations of motion are

$$x'' + k_x^{\text{sf}2} x = 0, \quad y'' + (ik_y^{\text{sf}})^2 y = 0, \quad (5)$$

For a pure quadrupole $k_x^{\text{sf}} = k_y^{\text{sf}} = k^{\text{sf}} \geq 0$. In the thin lens limit, for a lens of length L ,

$$q_x^{\text{sf}} = \frac{1}{f_x^{\text{sf}}} = k^{\text{sf}} \sin k^{\text{sf}} L, \quad q_y^{\text{sf}} = \frac{1}{f_y^{\text{sf}}} = -k^{\text{sf}} \sin k^{\text{sf}} L. \quad (6)$$

The general solutions of Eqs. (5) are

$$\begin{aligned} x(z) &= c_1 \cos k^{\text{sf}} z + d_1 \sin k^{\text{sf}} z \\ y(z) &= c_2 \cos ik^{\text{sf}} z - id_2 \sin ik^{\text{sf}} z = c_2 \cosh k^{\text{sf}} z + d_2 \sinh k^{\text{sf}} z. \end{aligned} \quad (7)$$

Expressed in terms of transfer matrices

$$\begin{pmatrix} x \\ x' \\ \Delta \end{pmatrix} = \begin{pmatrix} c_x & s_x & 0 \\ -s_x k^{\text{sf}2} & c_x & 0 \\ 0 & 0 & 1 \end{pmatrix} \begin{pmatrix} x_0 \\ x'_0 \\ \Delta_0 \end{pmatrix}, \quad (8)$$

$$\begin{pmatrix} y \\ y' \end{pmatrix} = \begin{pmatrix} c_y & s_y \\ s_y k^{\text{sf}2} & c_y \end{pmatrix} \begin{pmatrix} y_0 \\ y'_0 \end{pmatrix}, \quad (9)$$

where

$$c_x = \cos k^{\text{sf}} z, \quad s_x = \frac{\sin k^{\text{sf}} z}{k^{\text{sf}}}, \quad c_y = \cosh k^{\text{sf}} z, \quad s_y = \frac{\sinh k^{\text{sf}} z}{k^{\text{sf}}}. \quad (10)$$

The longitudinal offset coordinate Δ will be discussed later.

For small z the 1,2 elements reduce to the immediate drift length z and the 2,1 components reduce to the inverse focal length ascribable to length z . For a vertically focusing quad the sines and cosines are replaced by sinh and cosh functions, and the sign of the 2,1 element is reversed.

2.3 Achievable Electrostatic Quadrupole Focusing Strength

For magnetic quadrupoles the quadrupole focal length can be made very small, thereby permitting short cell length and small beta functions. For electrostatic quadrupoles it will not be possible to reduce the focal length below some minimum value (at the required proton momentum.) On the other hand, because of simpler construction and less space wastage at element ends it may be economical for L_{cell} to be smaller than would be optimal with magnets. This makes it appropriate to design electrostatic quadrupoles having the highest possible field gradient consistent with electrode separation equal to the gap width g of the lattice steering elements.

According to Eq. (3) the focal length of a pEDM electrostatic half-quadrupole of length l_Q is

$$f_x = \frac{\beta pc/e}{V_Q} \frac{g_Q^2}{8} \frac{1}{l_Q} \left(\text{e.g. } \frac{0.6 \times 0.7 \text{ GV}}{2V_Q/g_{\text{min.}}} \frac{0.02 \text{ m } (g_Q/g_{\text{min.}})}{4} \frac{1}{l_Q} \right) \quad (11)$$

To facilitate the following numerical estimate, both numerator and denominator have been divided by $g_{\text{min.}}$ which is the minimum distance between electrodes as shown in Fig. 2. Also one g_Q factor has been set to 0.02 m, which matches the quadrupole aperture to the nominal bending element aperture g . One can conjecture that the maximum possible electric field value in the quadrupole will be approximately the same as the maximum possible field value in the sector bending element. (This is conservative, since the minimum gap in a quadrupole is much less than the accelerator bore diameter, and reducing the electrode separation makes it easier to support a given electric field.) Based on nothing more than the appearance of Fig. 2, which was drawn by eyeball, the value of the ratio $g_Q/g_{\text{min.}}$ may be about 3.5. Using the peak field value of

15 MV/m would give $2V_Q/g_{\min.} = 15 \text{ MeV/m}$, $2V_Q = 86 \text{ kV}$, or $V_Q = \pm 42.9 \text{ kV}$, and $dE_x/dx = 8V_Q/g_Q^2 = 0.86 \text{ GV/m}^2$.

A private communication from Bill Morse estimates the achievable value of dE_x/dx to be 0.90 GV/m^2 , close to the value just estimated. (The agreement at this level is somewhat fortuitous, since he used a different quadrupole design and $g_Q = 3 \text{ cm}$ instead of $g_Q = 2 \text{ cm}$.) Bill then shows that this is large enough (with a safety margin of 1.7), to meet the quadrupole strength requirements assumed in the Pedm R&D plan dated (6/09). (In particular, full quadrupole length $2\ell_Q = 0.38 \text{ m}$ was assumed.)

Returning to Eq. (11), for given l_Q , the minimum quadrupole focal length is estimated to be

$$f_{x,\min.} \approx \frac{0.6 \times 0.7 \text{ GV}}{15 \text{ MV/m}} \frac{0.02 \text{ m} \times 3.5}{4} \frac{1}{l_Q} = \frac{1}{K_{1,\max.} l_Q} = \frac{0.49 \text{ m}^2}{l_Q} \quad (12)$$

Specific to the proton EDM “magic” momentum, the constraint on quadrupole field gradient can be expressed as

$$|K_1| < K_{1,\max.} = 2.04 \text{ m}^{-2}. \quad (13)$$

For an equal tune FODO lattice with cell length L_{cell} , and typical phase advance per cell, the half-quadrupole focal length is $f = L_{\text{cell}}/\sqrt{2}$. As an example, with $L_{\text{cell}} = 6 \text{ m}$, the minimal half-quadrupole length is $l_{Q,\min.} = 0.12 \text{ m}$. With each full cell containing two full quads, the quadrupoles take up about ten percent of the longitudinal space. This seems acceptably small, but it suggests that L_{cell} cannot be reduced much below 6 m. And, later, when unequal tune lattices are investigated, values of L_{cell} greater than 6 m may be needed.

For lattice design it is convenient to treat separated function quadrupoles as thin lenses while, at the same time, allotting just enough longitudinal space for the actual thick element. To minimize the quadrupole length ℓ_Q one must maximize the quadrupole strength coefficient. For given lens strength $q \equiv 1/f$ one then obtains

$$l_{Q,\min.} = \frac{q}{K_{1,\max.}} \left(\stackrel{\text{e.g.}}{\equiv} 0.49 \text{ m}^2 q \text{ for pEDM} \right). \quad (14)$$

The discussion has made no allowance whatsoever for a limitation emphasized by Bennett, et al. In order to avoid the build up of trapped electrons, they pulsed the electric quadrupoles on only briefly. This would probably be unworkable for the EDM experiment. But, since there will be no superimposed magnetic field, this particular failure mechanism should be absent. Nevertheless there may be other failure modes, such as sparking induced by stray protons.

3 Unequal Tune FODO Lattice Design

In practice the capability of having greatly different horizontal and vertical tunes is usually not needed and standard formulas for FODO lattices have equal horizontal and vertical phase advances. But the proton EDM experiment probably

favors horizontal tune greater than vertical tune. (This gives increased BPM sensitivity needed for accurately matching the vertical positions of the counter-circulating beams). Appropriately generalized formulas are therefore needed. Inverse focal lengths are to be denoted by $q \equiv 1/f$. *Positive* q corresponds to *focusing* in the x -plane (*horizontal*).

Cell parameters are indicated in Fig. 3. The cell half-length (distance between adjacent lens centers) is l . Thin lens half-quadrupoles with strengths $q_1 \equiv 1/f_1$ and $q_2 \equiv 1/f_2$, are located at positions indicated 1 and 2 in the figure. One of q_1 and q_2 will be positive, the other negative. A (negative) bend through angle $\Delta\theta$ is assumed to occur at the center of each half cell. By working with half-quads, lattice functions will be obtained at quadrupole centers. This is especially convenient for periodic lattices since the (Twiss) beta function slopes $\beta'_x \equiv -2\alpha_x$ and $\beta'_y \equiv -2\alpha_y$ then vanish at quad centers. Thin sextupoles of strength S_1 or S_2 are centered between the half quads. This preserves clockwise-counterclockwise symmetry. To simplify the linear model the quadrupole and sextupole thicknesses, and their adjacent straight section lengths are all neglected. These sextupoles are treated as half sextupoles to make their center points accessible (in the lattice model) but there would actually be a single unit.

The x transfer matrix $2 \leftarrow 1$ is

$$M_{21}^{(x)} = \begin{pmatrix} 1 & 0 \\ -q_2 & 1 \end{pmatrix} \begin{pmatrix} 1 & l \\ 0 & 1 \end{pmatrix} \begin{pmatrix} 1 & 0 \\ -q_1 & 1 \end{pmatrix} = \begin{pmatrix} 1 - q_1 l & l \\ -q_1 - q_2 + q_1 q_2 l & 1 - q_2 l \end{pmatrix}, \quad (15)$$

and a similar matrix for $1 \leftarrow 2$ is obtained by switching q_1 and q_2 . The full cell, $1 \leftarrow 1$, x -transfer matrix is

$$M_{11}^{(x)} = \begin{pmatrix} 1 - q_2 l & l \\ -q_1 - q_2 + q_1 q_2 l & 1 - q_1 l \end{pmatrix} \begin{pmatrix} 1 - q_1 l & l \\ -q_1 - q_2 + q_1 q_2 l & 1 - q_2 l \end{pmatrix} \\ = \begin{pmatrix} 1 - 2q_1 l - 2q_2 l + 2q_1 q_2 l^2 & 2l(1 - q_2 l) \\ 2(-q_1 - q_2 + q_1 q_2 l)(1 - q_1 l) & 1 - 2q_1 l - 2q_2 l + 2q_1 q_2 l^2 \end{pmatrix}. \quad (16)$$

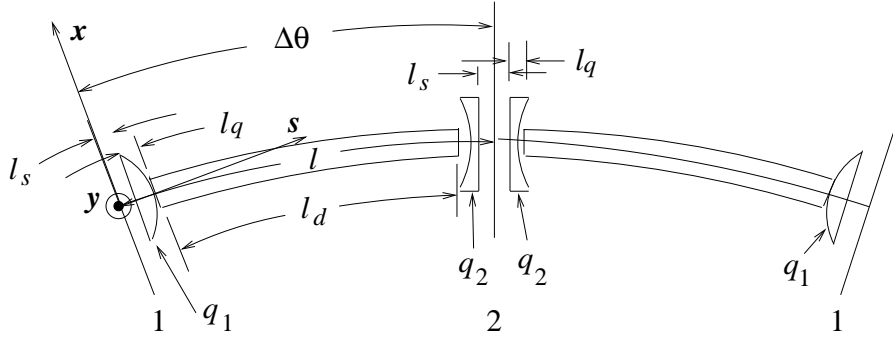


Figure 3: Thin lens, separated function electrostatic FODO lattice, showing dimensioning and element strength parameters. Sextupoles are not shown.

For a periodic lattice made by repeating these cells, this matrix can be written in ‘‘Twiss’’ form, with α vanishing, as stated previously;

$$M_{11}^{(x)} = \begin{pmatrix} \cos \mu^{(x)} & \beta^{(x)} \sin \mu^{(x)} \\ -\sin \mu^{(x)}/\beta^{(x)} & \cos \mu^{(x)} \end{pmatrix}. \quad (17)$$

Equating coefficients and generalizing to include y motion by switching the signs of q_1 and q_2 leads to

$$\begin{aligned} C^{(x)} = \cos \mu^{(x)} &= 1 - 2q_1l - 2q_2l + 2q_1q_2l^2, & \sin^2 \frac{\mu^{(x)}}{2} &= q_1l + q_2l - q_1q_2l^2, \\ C^{(y)} = \cos \mu^{(y)} &= 1 + 2q_1l + 2q_2l + 2q_1q_2l^2, & \sin^2 \frac{\mu^{(y)}}{2} &= -q_1l - q_2l - q_1q_2l^2. \end{aligned} \quad (18)$$

For the lattice to be stable, both cosine magnitudes have to be less than 1.

The β -functions are obtained similarly;

$$\begin{aligned} \beta_1^{(x)} &= l \sqrt{\frac{1 - q_2l}{1 - q_1l}} \sqrt{\frac{1}{q_1l + q_2l - q_1q_2l^2}} = l \sqrt{\frac{1 - q_2l}{1 - q_1l}} \sqrt{\frac{2}{1 - C^{(x)}}} = \sqrt{\frac{1 - q_2l}{1 - q_1l}} \frac{l}{\sin \frac{\mu^{(x)}}{2}}, \\ \beta_1^{(y)} &= l \sqrt{\frac{1 + q_2l}{1 + q_1l}} \sqrt{\frac{1}{-q_1l - q_2l - q_1q_2l^2}} = l \sqrt{\frac{1 + q_2l}{1 + q_1l}} \sqrt{\frac{2}{1 - C^{(y)}}} = \sqrt{\frac{1 + q_2l}{1 + q_1l}} \frac{l}{\sin \frac{\mu^{(y)}}{2}}, \\ \beta_2^{(x)} &= l \sqrt{\frac{1 - q_1l}{1 - q_2l}} \sqrt{\frac{1}{q_1l + q_2l - q_1q_2l^2}} = l \sqrt{\frac{1 - q_1l}{1 - q_2l}} \sqrt{\frac{2}{1 - C^{(x)}}} = \sqrt{\frac{1 - q_1l}{1 - q_2l}} \frac{l}{\sin \frac{\mu^{(x)}}{2}}, \\ \beta_2^{(y)} &= l \sqrt{\frac{1 + q_1l}{1 + q_2l}} \sqrt{\frac{1}{-q_1l - q_2l - q_1q_2l^2}} = l \sqrt{\frac{1 + q_1l}{1 + q_2l}} \sqrt{\frac{2}{1 - C^{(y)}}} = \sqrt{\frac{1 + q_1l}{1 + q_2l}} \frac{l}{\sin \frac{\mu^{(y)}}{2}}. \end{aligned} \quad (19)$$

Note the simple identities,

$$\sqrt{\beta_1^{(x)}\beta_2^{(x)}} = \frac{l}{\sin \frac{\mu^{(x)}}{2}}, \quad \sqrt{\beta_1^{(y)}\beta_2^{(y)}} = \frac{l}{\sin \frac{\mu^{(y)}}{2}}. \quad (20)$$

and

$$\frac{\beta_1^{(x)}}{\beta_2^{(x)}} = \frac{1 - q_2l}{1 - q_1l}, \quad \frac{\beta_1^{(y)}}{\beta_2^{(y)}} = \frac{1 + q_2l}{1 + q_1l}. \quad (21)$$

Often $\mu^{(x)}$ and $\mu^{(y)}$ are approximately equal. If they are exactly equal, the formulas simplify considerably. Taking point 1 to be a horizontally focusing quadrupole location we define

$$q_1 = -q_2 = |q|, \quad (22)$$

and obtain

$$\cos \mu = 1 - 2|q|^2l^2, \quad \sin \frac{\mu}{2} = |q|l, \quad (23)$$

as well as the relations,

$$\begin{aligned}\beta_1^{(x)} &= \sqrt{\frac{1+|q|l}{1-|q|l}} \frac{1}{|q|}, & \beta_1^{(y)} &= \sqrt{\frac{1-|q|l}{1+|q|l}} \frac{1}{|q|}, \\ \beta_2^{(x)} &= \sqrt{\frac{1-|q|l}{1+|q|l}} \frac{1}{|q|} = \beta_1^{(y)}, & \beta_2^{(y)} &= \sqrt{\frac{1+|q|l}{1-|q|l}} \frac{1}{|q|} = \beta_1^{(x)}\end{aligned}\quad (24)$$

Then Eqs. (24) reduce to

$$\beta_1^{(x)} \beta_2^{(x)} = \beta_1^{(y)} \beta_2^{(y)} = f^2. \quad (25)$$

For designing unequal tune lattices one can divide the first of Eqs. (20) by the second to obtain

$$\frac{\beta_1^{(x)} \beta_2^{(x)}}{\beta_1^{(y)} \beta_2^{(y)}} = \frac{\sin^2 \frac{\mu^{(y)}}{2}}{\sin^2 \frac{\mu^{(x)}}{2}} = \frac{-q_1 - q_2 - q_1 q_2 l}{q_1 + q_2 - q_1 q_2 l} \stackrel{\text{e.g.}}{=} \frac{1}{B^2}, \quad (26)$$

where Eq. (18) was used to eliminate the trigonometric ratio, and B^2 is perhaps a big number, such as 10. Solving the last of Eqs. (26) yields

$$f_1 = -f_2 - \frac{B^2 - 1}{B^2 + 1} \ell. \quad (27)$$

This formula gives the deviation from equality of focal length f_1 from $-f_2$ needed to produce a given ratio B . The factor B can be thought of as a beta function ratio or, via Eq. (26), as monotonically related to a tune ratio. B becomes erratically large as the value of the final term approaches ℓ . To achieve an unbalanced lattice for which the optics remains reasonably under control one can try opposite sign, equal magnitude deviations. Empirically it seems more rapidly convergent to first strengthen the quad that focuses in the plane needing higher tune, while leaving the other quad unchanged.

Choosing $B > 1$ reduces the focal length of the horizontally focusing quad at location 1 (i.e. stronger horizontal focusing). In what follows the parameter B will be generalized as a fudge factor quantifying various aperture-limiting effects.

3.1 Longitudinal Variation of the Lattice Functions

In the drift regions between quadrupoles the β -functions vary quadratically with s . At the quad center the slope $\beta' = d\beta/ds \equiv -2\alpha$ vanishes, but there are slope discontinuities related to the quad strengths by

$$\Delta\beta'^{(x)} = -2q_1\beta_1^{(x)}, \quad \Delta\beta'^{(y)} = 2q_1\beta_1^{(y)}, \quad (28)$$

so the Twiss parameters at the quadrupole exit are given by

$$\begin{aligned}\alpha_{1+}^{(x)} &= q_1\beta_1^{(x)}, & \alpha_{1+}^{(y)} &= -q_1\beta_1^{(y)}, \\ \gamma_{1+}^{(x)} &= \frac{1 + q_1^2(\beta_1^{(x)})^2}{\beta_1^{(x)}}, & \gamma_{1+}^{(y)} &= \frac{1 + q_1^2(\beta_1^{(y)})^2}{\beta_1^{(y)}}.\end{aligned}\quad (29)$$

In the region from 1 to 2 the β -functions vary as

$$\beta^{(x)}(s) = \beta_1^{(x)} - 2\alpha_{1+}^{(x)}s + \gamma_{1+}^{(x)}s^2, \quad \beta^{(y)}(s) = \beta_1^{(y)} - 2\alpha_{1+}^{(y)}s + \gamma_{1+}^{(y)}s^2. \quad (30)$$

The slope of the horizontal dispersion function $\tilde{D}(s)$ vanishes at the quadrupole center, but there is a slope discontinuity at 1, due to the quadrupole, such that

$$\tilde{D}'_{1+} = -q_1\tilde{D}_1, \quad (31)$$

and a slope discontinuity $\Delta\theta$ at $l/2$ due to the bend (which is being treated as if concentrated at the center of the half cell). As a result, the value of \tilde{D}_2 is

$$\tilde{D}_2 = \tilde{D}_1 - q_1\tilde{D}_1l + \Delta\theta\frac{l}{2}, \quad \tilde{D}_1 = \tilde{D}_2 - q_2\tilde{D}_2l + \Delta\theta\frac{l}{2}, \quad (32)$$

where the same argument has given the second equation also. Solving Eq. (32) yields

$$\tilde{D}_1 = \frac{(1 - q_2l/2)l\Delta\theta}{\sin^2\frac{\mu^{(x)}}{2}}, \quad \tilde{D}_2 = \frac{(1 - q_1l/2)l\Delta\theta}{\sin^2\frac{\mu^{(x)}}{2}}. \quad (33)$$

For the case of equal tunes as in Eq. (22) these become

$$\tilde{D}_1 = \frac{(1 + |q|l/2)l\Delta\theta}{|q|l^2}, \quad \tilde{D}_2 = \frac{(1 - |q|l/2)l\Delta\theta}{|q|l^2}, \quad (34)$$

with the useful consequence that

$$\frac{\tilde{D}_1 + \tilde{D}_2}{2} = \frac{\Delta\theta}{lq^2}. \quad (35)$$

3.2 Setting the Tunes

One can adjust the strengths q_1 and q_2 to achieve desired values for the phase advances $\mu^{(x)}$ and $\mu^{(y)}$. Defining the ‘‘average’’ quantity

$$\overline{\mathcal{S}^2} = \frac{1}{2}\left(\sin^2\frac{\mu^{(x)}}{2} + \sin^2\frac{\mu^{(y)}}{2}\right), \quad (36)$$

and the ‘‘difference’’ quantity,

$$\Delta(\mathcal{S}^2) = \sin^2\frac{\mu^{(y)}}{2} - \sin^2\frac{\mu^{(x)}}{2}, \quad (37)$$

Eqs. (18) become

$$q_1l + q_2l = -\Delta(\mathcal{S}^2)/2, \quad q_1lq_2l = -\overline{\mathcal{S}^2}. \quad (38)$$

These lead to the quadratic equation

$$(q_1l)^2 + \frac{1}{2}\Delta(\mathcal{S}^2)q_1l - \overline{\mathcal{S}^2} = 0, \quad (39)$$

with the roots being

$$q_1l = \pm\sqrt{\overline{\mathcal{S}^2} + (\Delta(\mathcal{S}^2))^2/16} - \Delta(\mathcal{S}^2)/4. \quad (40)$$

The sign choice depends upon which of the two quads is horizontally focusing— for FODDOF $q_1 > 0, q_2 < 0$, for DOFFOD $q_1 < 0, q_2 > 0$.

3.3 Compensation For Dipole Focusing

The tune shift caused by a small quadrupole perturbation. A result that is so important in accelerator physics that it deserves to be called “the golden rule” is that a quadrupole perturbation of strength Δq , at a point in the lattice where the beta-functions are β_x and $\beta^{(y)}$, causes tune shifts given by

$$\Delta\nu_x = \frac{1}{4\pi}\beta_x\Delta q, \quad \Delta\nu_y = -\frac{1}{4\pi}\beta_y\Delta q. \quad (41)$$

For positive q the horizontal tune is shifted to higher value. The same quad shifts the vertical tune to lower value.

Use of the golden rule to compensate for dipole focusing. There is a focusing effect due a dipole, say a sector bend, that shifts the horizontal tune. Especially in small rings, compensating for this shift improves agreement between desired and achieved tunes. Assume that the magnet lengths satisfy

$$l_d + l_q + l_s = l. \quad (42)$$

The effective focusing strength of the dipole (it acts only in the horizontal plane) is

$$q_d = \frac{(\Delta\theta)^2}{l_d}. \quad (43)$$

This quadrupole perturbation shifts the tune by an amount

$$\Delta\nu^{(x)} = \frac{n}{4\pi}q_d\overline{\beta^{(x)}} = \frac{n}{2\pi}(\Delta\theta)^2\frac{l/l_d}{\sin\frac{\mu^{(x)}}{2}}. \quad (44)$$

where $\overline{\beta^{(x)}}$ has been approximated using Eq. (20) and q_d taken from Eq. (43). This tune shift is necessarily positive. To compensate for this perturbation, which to this point has been neglected, we apply changes Δq_1 and Δq_2 to q_1 and q_2 , applying the condition that both total tune shifts vanish yields

$$\begin{aligned} 4\pi\Delta\nu_1^{(x)} = 0 &= \Delta q_1\beta_1^{(x)} + \Delta q_2\beta_2^{(x)} + q_d\overline{\beta^{(x)}}, \\ 4\pi\Delta\nu_1^{(y)} = 0 &= -\Delta q_1\beta_1^{(y)} - \Delta q_2\beta_2^{(y)}. \end{aligned} \quad (45)$$

Solving these equations yields

$$\Delta q_1 = -q_d\frac{\beta_2^{(y)}}{\beta_1^{(x)}\beta_2^{(y)} - \beta_1^{(y)}\beta_2^{(x)}}\frac{l}{\sin\frac{\mu^{(x)}}{2}}, \quad \Delta q_2 = -\Delta q_1\frac{\beta_1^{(y)}}{\beta_2^{(y)}}. \quad (46)$$

3.4 Beam Acceptance and Cell Length Determination

To proceed it is necessary to have at least a ball park estimate of the lattice cell length L_{cell} that will be required. The optimal phase advance per FODO cell depends on what is being optimized, but usually $\mu \approx \pi/2$. At that point,

recalling that $\ell = L_{\text{cell}}/2$ is the FODO cell half length, according to Eq. (23) the required lens focal length is

$$f = \frac{1}{q} = \sqrt{2}\ell = \frac{L_{\text{cell}}}{\sqrt{2}}. \quad (47)$$

The experiment depends critically upon the emittances ϵ_x and ϵ_y of the proton beam; in terms of them the beam sizes σ_x and σ_y are given by $\sqrt{\beta_x\sigma_x}$ and $\sqrt{\beta_y\sigma_y}$. Let us take $\epsilon = \sqrt{\epsilon_x\epsilon_y}$ for both emittances. This will be most valid in the (likely) case that the emittances are approximately equal.

Alexei Fedotov[3] has given $\epsilon_{n,95} = 5 - 6 \mu\text{m}$ as a tentative normalized emittance containing 95% of the particles. With $\beta = 0.60$ and $\gamma = 1.25$, the lower value corresponds to unnormalized emittance $\epsilon_{95} = \epsilon_{n,95}/(\beta\gamma) = 6.7 \mu\text{m}$. Fedotov also states that the rms emittance is related to the unnormalized emittance by $\epsilon_{95} = 6\sigma^2/\beta$. Expressed in terms of a corresponding beam size $\sigma = \sqrt{\sigma_x\sigma_y}$ at a point where the horizontal and vertical sizes are equal, and using Eqs. (25) and (47) to estimate the parameters, gives

$$\sigma \approx \sqrt{f\epsilon_{95}/6} \approx \sqrt{\frac{L_{\text{cell}}\epsilon_{95}/6}{\sqrt{2}}}, \quad \left(\text{e.g. } \sqrt{L_{\text{cell}} \times 0.80 \times 10^{-6} \text{ m.}} \right). \quad (48)$$

The aperture requirements are somewhat different horizontally and vertically. It is typical for momentum spread and betatron oscillations to contribute more or less equally to horizontal beam size. One can introduce an (effective beta function multiplier) factor $B^{(H)} \approx 4$ to express this. The main vertical aperture effect was expressed earlier by the factor B , which we now re-christen as $B^{(V)}$, so that B can stand for the larger of $B^{(H)}$ and $B^{(V)}$. At this stage B can be thought of as a ‘‘fudge factor’’, present to allow for beam size increasing effects already mentioned, or others.

Continuing to let σ stand for either σ_x or σ_y , one requires σ to be less than the electrode half gap $g/2$ by some numerical factor $\eta_{\text{stay clear}}$. For the EDM experiment one expects to be intentionally scraping some beam on injection, so a value $\eta_{\text{stay clear}}$ as small as 1, may be acceptable. Allowing for the various limitations yields

$$\frac{g}{2} > \eta_{\text{stay clear}} \sqrt{B} \sqrt{\frac{L_{\text{cell}}\epsilon_{95}/6}{\sqrt{2}}} \quad (49)$$

Expressed as a maximum cell length, this yields

$$L_{\text{cell}} > \frac{g^2}{\epsilon_{95}} \frac{2.1}{\eta_{\text{stay clear}}^2 B}. \quad (50)$$

For the tunnel circumference to be acceptably small the gap g has been specified to not exceed 2 cm. Using $B = 4$ and $\eta_{\text{stay clear}} = 2$ yields maximum cell length $L_{\text{cell}} = 7.8 \text{ m}$.

The numerical coefficient here, especially the factor B , is not reliable here. But this formula suggests how the maximum cell length depends on other parameters. Eq. (50) provides an upper acceptable bound for the cell length and

Eq. (12) implies a lower achievable bound. In an optimal design these two values will be approximately equal.

4 Combined Function Electrostatic Bending Elements

4.1 Field Calculation

Another approach to allowing strongly unbalanced tunes is to provide the vertical focusing by combined-function, toroidally-shaped steering electrodes. From the earlier discussion of FODO lattices with vertical tune much less than horizontal, it seems clear that vertical aperture restriction in the vertical focusing quadrupoles may impose a fundamental limitation. Making the vertical focusing quadrupoles longer (so they can have larger apertures) relieves the problem. Carrying this to the extreme, we next build vertical focusing into *all* of the bending elements.

A characteristic of accelerator magnets is that they are easily accessible from the side, for example for beam injection or extraction. For the same reason it is relatively easy to provide generous horizontal aperture in magnets. Electric bending elements, on the other hand, are more naturally accessible from above or below. Also, with the dominant bending provided by vertical plates, vertical aperture is easy to provide, horizontal not. This will remain true even if the bending elements are curved to provide vertical focusing. The advantage will, to some extent, be compromised by vertical aperture limitation in the strong, separated-function, horizontal focusing quadrupoles that are necessarily present in the lattice. One will have to check that their acceptance is greater than other obstacles, such as polarimeters or injection or extraction septa.

To provide vertical focusing in weak focusing magnetic accelerators the magnet poles are shaped to cause the magnetic field to fall off with increasing radius—the field index n in the field dependence $B_y \sim (r_0/r)^n$ is positive (but smaller than 1 for horizontal stability.) In a combined function, strong focusing, alternating gradient accelerator some magnets have positive n , some negative, but “strong” implies the magnitude of n is much greater than 1 in both cases. For the proton EDM candidate lattice to be discussed here, the only combined function bends will be vertically focusing and strong, so the electrostatic parameter analogous to n will be large and positive. This is helpful to keep in mind as the signs are very confusing.

Electrodes to provide electrostatic bending, as well as focusing are shown in Fig. 4. A simplification that makes analytic field calculation possible is to assume the electrodes are circular cylinders projecting normally out of the plane of the paper. In practice the electrodes will be toroidal in shape. The approximation will be good when the major bending radius r_0 is much greater than the minor radii R_1 and R_2 of the inner and outer electrodes respectively. As drawn the electrodes are complete cylinders, osculating at the point O, diametrically opposite to the design orbit position. In fact the electrodes will be truncated

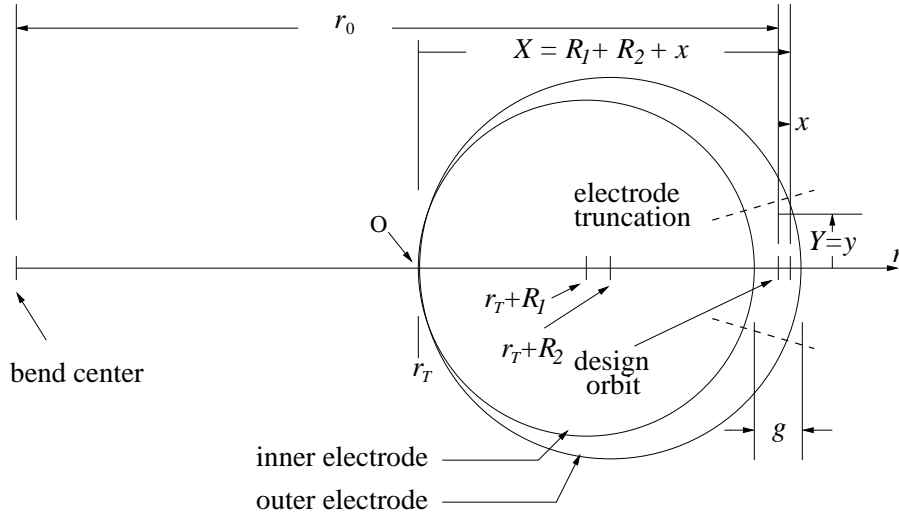


Figure 4: Combined-function, eccentric-cylinder, electrostatic electrodes proposed for proton EDM experiment. The electrodes will, in fact, be truncated, for example along the broken lines.

roughly as shown.

For 2D geometry the electric field can be calculated using conformal mapping. Following Kober[1], the calculation can be based on the geometry shown in Fig. 5. In the $w = u + iv$ plane the electric field is that of two parallel plates, labeled P_1 and P_2 . In this geometry the electric potential ϕ is a linear function of (real part) u . An analytic transformation from w to $Z = X + iY$ maps equipotentials to equipotentials. In this case one seeks a transformation which transforms the planes P_1 and P_2 to the inner and outer cylindrical electrodes. From Kober the complex transformation accomplishing this is

$$w = u_1 + \left(\frac{u_2 - u_1}{2(R_2 - R_1)} \right) 2R_2 \frac{Z - 2R_1}{Z}. \quad (51)$$

Here, with $g = 2(R_2 - R_1)$ being the central separation gap of the electrodes, the expression in large parentheses is $-E_{\text{nom.}}$, the (negative) nominal electric field between the plates (treated as planes.) Taking $\phi = \Re(w)$ as the electric potential yields

$$\phi(X, Y) = U_1 - 2E_{\text{nom.}}R_2 \left(1 - \frac{2R_1X}{X^2 + Y^2} \right). \quad (52)$$

in terms of displacement x from the design orbit,

$$X = R_1 + R_2 + x, \quad (53)$$

and the potential is

$$\phi(x, y) = U_1 - 2E_{\text{nom.}}R_2 \left(1 - \frac{2R_1(R_1 + R_2 + x)}{(R_1 + R_2 + x)^2 + y^2} \right). \quad (54)$$

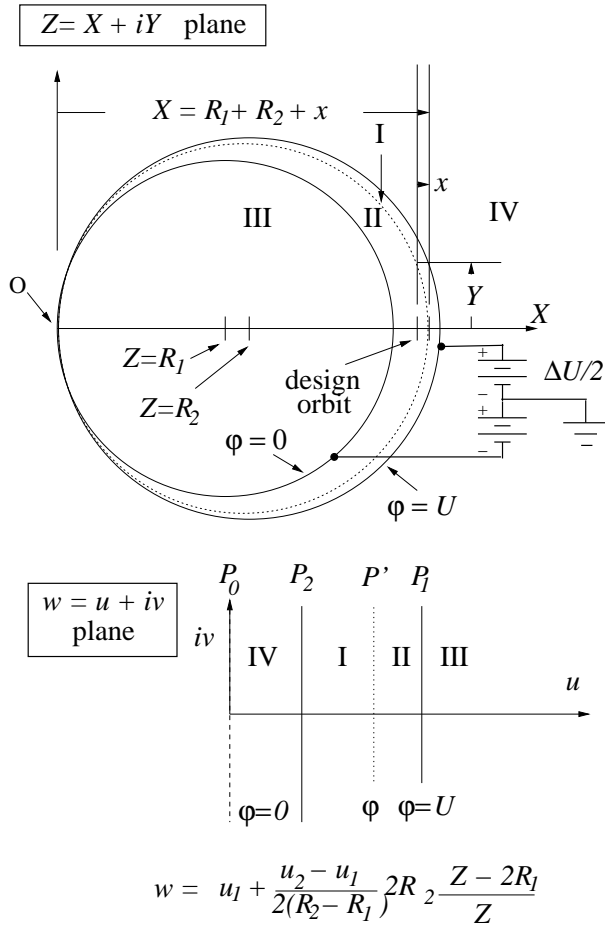


Figure 5: Conformal transformation from “parallel plate electric field” to electric field in region between osculating eccentric circles.

In the horizontal plane (containing the design orbit) the electric field, $E_x = -\partial\phi/\partial x$, is given by

$$E_x(x, y = 0) = E_{\text{nom.}} \frac{4R_1R_2}{(R_1 + R_2)^2} \left(1 - \frac{2x}{R_1 + R_2} + \frac{3x^2}{(R_1 + R_2)^2} + \dots \right) \quad (55)$$

It seems useful to introduce an average radius \bar{R} , and re-write this using the formulas

$$R_1 = \bar{R} - \frac{g}{2}, \quad R_2 = \bar{R} + \frac{g}{2}. \quad (56)$$

The result is

$$E_x(x, y = 0) = E_{x0} \left(1 - \frac{x}{\bar{R}} + \frac{3}{4} \frac{x^2}{\bar{R}^2} - \frac{1}{2} \frac{x^3}{\bar{R}^3} + \dots \right), \quad (57)$$

where, to suppress a factor whose deviation from 1 will certainly be small and may be negligible, a newly-nominal electric field

$$E_{x0} \equiv E_{\text{nom.}} \left(1 - \frac{1}{16} \frac{g^2}{\bar{R}^2} \right) \quad (58)$$

has been introduced. The (assumed to be positive) curvature of a proton with momentum p is given by

$$\frac{1}{r_0} = -\frac{E_r}{\beta pc/e}. \quad (59)$$

For inward (in the $-x$ direction) acceleration, E_r will be negative. Then, in thin element approximation, the bend angle in an element of length L is given by

$$\Delta\theta^{(E)}(x, y = 0) = -\frac{L}{r_0} \left(1 - \frac{x}{\bar{R}} + \frac{3}{4} \frac{x^2}{\bar{R}^2} - \frac{1}{2} \frac{x^3}{\bar{R}^3} + \dots \right). \quad (60)$$

Since this formula was calculated using 2D geometry, it is only an approximation to the true toroidal field. More accurate coefficients in the series may have to be calculated numerically.

4.2 Chromatic Deflection

This formula has described the deflection of an on-momentum particle of momentum p_0 . In a particle tracking program a general particle has momentum $p_0 + \Delta p$. The horizontal orbit equation of Eq. (4) can be augmented to account for this deviation, assuming, for now, that $x = 0$;

$$\left. \frac{d^2x}{dz^2} \right|_{x=0} = \frac{d}{dz} \frac{dx}{dz} = \frac{d}{dz} \frac{p_x}{p} \approx \frac{1}{p} \frac{dp_x}{dz} \approx \frac{eE_x}{pv}. \quad (61)$$

The longitudinal deviation variable δ used in MAD and UAL is defined by

$$\delta = \frac{\Delta\mathcal{E}}{p_0c} = \frac{m_0c^2\Delta\gamma}{p_0c}. \quad (62)$$

One then finds

$$\Delta(pv) = m_0\Delta(\gamma v^2) = m_0c^2\Delta\left(\gamma - \frac{1}{\gamma}\right) = \left(1 + \frac{1}{\gamma_0^2}\right) \frac{p_0v_0}{\beta_0} \delta, \quad (63)$$

and

$$pv \approx p_0v_0 \left(1 + \left(1 + \frac{1}{\gamma_0^2}\right) \frac{1}{\beta_0} \delta.\right) \quad (64)$$

Substitution into Eq. (61) yields

$$\left.\frac{d^2x}{dz^2}\right|_{x=0} = -\frac{1}{r_0} + \frac{1}{r_0} \left(1 + \frac{1}{\gamma_0^2}\right) \frac{1}{\beta_0} \delta. \quad (65)$$

This is the equation of motion for x treated as a Cartesian coordinate. It includes the design bending force. But we are only looking for the radial acceleration ascribable to the offset δ . We therefore suppress the first term to obtain

$$\left.\frac{d^2x}{dz^2}\right|_{x=0} = \frac{1}{r_0} \left(1 + \frac{1}{\gamma_0^2}\right) \frac{1}{\beta_0} \delta \equiv \frac{\Delta}{r_0}. \quad (66)$$

The fractional stiffness deviation Δ relates the radius of curvature r of a deviant particle to the radius of curvature r_0 of an on-momentum particle, both in the same uniform field;

$$r = r_0 (1 + \Delta). \quad (67)$$

Δ is related to the MAD/UAL momentum deviation factor δ by²

$$\Delta = \left(1 + \frac{1}{\gamma_0^2}\right) \frac{1}{\beta_0} \delta \quad (= 2.744 \delta \quad \text{for the proton EDM experiment.}) \quad (68)$$

5 Thin Element Representation of Electrostatic Bend/Lens

Unlike in a magnetic field, the speed of a particle is *not* preserved in an electrostatic element. Depending on transverse displacement, a proton slows down or speeds up as it enters the element. We wish, nevertheless, to treat the electrostatic bend/lens element as a thin element (even if the element is “thin” only by virtue of being one of the many slices of an element that is actually “thick”.) In this approximation the input, output, and central values of x are all the same for any single slice. (Of course x can change in the drift section between slices.)

For an isolated element, since the electric potential before entry, which we take to be zero, is equal to the potential after exiting (except for possible exit-entrance position deviation) the particle speed can be treated as (externally) conserved. For self-consistency it has to be assumed that acceleration changes

²For comparison with Wollnik’s Eq. (4.58c) one should note that Wollnik’s $\delta_K = (K - K_0)/K_0$ is a fractional kinetic energy, while our MAD/UAL $\delta = (E - E_0)/p_0c$. The numerators are the same but our denominator is bigger by $p_0c/K_0 = 3.01$.

the speed discontinuously at the input face, and restores the speed discontinuously at the output. In this approximation the magnitude of the particle's momentum, while the particle is between the plates, is a function only of its transverse displacement (x, y) , (or, to good approximation, just x .) The particle's deflection angle needs to be compensated accordingly for this “inertial” effect.

In the interior of a thick element, as the particle passes from one slice to the next, the particle has no possibility of returning to its external speed. But this does not matter, as its speed stays close to its current internal value on entering the next slice. (In the limit of infinitesimal slice thickness the speed is continuous.) When entering the first slice of an actually thick element, or when exiting the last slice, the effect of the actual fringe field has to be taken into account. As with magnetic pole-face rotation focusing, there is a focusing effect of non-normal entry. For now we assume normal entry. Adapting standard terminology, one can refer to the electrostatic device as a “sector bend”.

In a magnetic field the particle “stiffness” can be taken to be its momentum p . In an electric field, a consistent definition of stiffness is pv/c or, equivalently, p^2c/\mathcal{E} . In passing from outside to inside, both numerator and denominator change values, which is something of a nuisance.

For a particle with charge e , the total energy inside is

$$\mathcal{E}_{\text{inside}} \approx \mathcal{E}_{\text{outside}} + eE_{\text{nom.}} x. \quad (69)$$

(A proton with x positive will have less kinetic energy than with x negative because $E_{\text{nom.}}$ is negative—the electric field has to be centripetal.) We are assuming balanced electrode voltages as shown in Fig. 5, so the energy of a proton on the design orbit is unchanged upon entry. This simplifies the description of the design orbit. (If balanced voltages are experimentally inconvenient, small changes in the formulas will be required.) By incorporating the inertial effect into the focusing strength coefficients, the energy of each proton will ultimately be treated as a constant of motion everywhere. But, for now, the equations will have the proton kinetic energy correctly tracking the electric potential. For convenience we rearrange Eq. (69) to

$$\frac{\mathcal{E}_{\text{inside}}}{\mathcal{E}} \approx 1 + \frac{eE_{\text{nom.}} x}{\mathcal{E}} \quad (70)$$

where here, and from now on, we suppress the “outside” subscript. The total momentum inside satisfies

$$\begin{aligned} p_{\text{inside}}^2 c^2 &= (\mathcal{E} + eE_{\text{nom.}} x)^2 - m^2 c^4 \\ &\approx p^2 c^2 + 2eE_{\text{nom.}} \mathcal{E} x. \end{aligned} \quad (71)$$

To this approximation

$$\frac{p_{\text{inside}}^2}{p^2} = 1 + \frac{2eE_{\text{nom.}} \mathcal{E} x}{p^2 c^2} \quad (72)$$

Combining equations, we obtain

$$\frac{(p^2/\mathcal{E})_{\text{inside}}}{p^2/\mathcal{E}} \approx \frac{1 + \frac{2eE_{\text{nom.}}\mathcal{E}}{p^2c^2}x}{1 + \frac{eE_{\text{nom.}}}{\mathcal{E}}x} \approx 1 + \frac{eE_{\text{nom.}}}{\mathcal{E}} \left(\frac{2}{\beta^2} - 1 \right) x. \quad (73)$$

The presence of the final term shows that the particle deflection depends on x even if the radial electric field is independent of x . To account for this “inertial” effect, the fractional momentum offset δ could be augmented by the final term. Though physically faithful, this is somewhat inconvenient, since magnet-centric computer codes treat δ as a constant of motion (except in RF cavities.)

In practice, the radial electric field will intentionally be designed to have a component varying proportional to x . This will cause what will be referred to as a “field effect”, with the field being predominantly “quadrupole”. In what follows the formalism will be rearranged to subsume the inertial effect into the quadrupole strength parameter. Summing the inertial effect and the field effect, the focusing effect of an element can be represented by an (effective magnetic) quadrupole coefficient $K_{1,\text{eff.}}^{(E)}$. Calculation of the effective sextupole coefficient $K_{2,\text{eff.}}^{(E)}$ has to be worked out similarly.

6 Electric Parameterization Via Conventional Magnet Formalism

6.1 Matching to Conventional Formalism

In TRANSPORT notation, the magnetic field in the horizontal plane containing the design orbit is expressed as a series

$$B_y(x, y = 0) = B_{y0} \left(1 - n \frac{x}{r_0} + \beta \frac{x^2}{r_0^2} + \gamma \frac{x^3}{r_0^3} + \dots \right) \quad (74)$$

where the “field index” n is (therefore) defined by

$$n = - \frac{r_0}{B_{y0}} \left. \frac{\partial B_y}{\partial x} \right|_{x=0}, \quad (75)$$

where r_0 is the design orbit radius. Consider a sector bend magnet of (arc) length L . The curvature $1/r_0$ and the bend angle $\Delta\theta^{(M)}$ of a proton of momentum p are given by

$$\frac{1}{r_0} = \frac{cB_{y0}}{pc/e}, \quad \text{and} \quad \Delta\theta^{(M)} = -\frac{L}{r_0} = -\frac{cB_{y0}L}{pc/e}. \quad (76)$$

In MAD notation the same x -dependence is parameterized as

$$B_y(x, y = 0) = B_{y0} \left(1 + \frac{K_1 r_0}{1!} x + \frac{K_2 r_0}{2!} x^2 + \frac{K_3 r_0}{3!} x^3 + \dots \right). \quad (77)$$

Matching formulas we have, for example,

$$K_1 = -\frac{n}{r_0^2}, \quad K_2 = \frac{2\beta}{r_0^3}. \quad (78)$$

In thin element approximation the bend angle is

$$\Delta\theta^{(M)}(x, y = 0) = \frac{cB_{y0}L}{pc/e} \left(1 + \frac{K_1 r_0}{1!} x + \frac{K_2 r_0}{2!} x^2 + \frac{K_3 r_0}{3!} x^3 + \dots \right). \quad (79)$$

For counter-clockwise (from above) orbit rotation, to make $\Delta\theta^{(M)}$ be negative requires $B_y < 0$. Matching coefficients in Eqs. (60) and (79), we can define parameters

$$K_1^{(E,\text{field})} = -\frac{1}{\bar{R}r_0}, \quad K_2^{(E,\text{field})} = \frac{3}{2\bar{R}^2 r_0}, \quad K_3^{(E,\text{field})} = -\frac{3}{\bar{R}^2 r_0}, \quad \dots \quad (80)$$

The superscripts here include ‘‘field’’ as a reminder that these parameters include neither the inertial effect nor the toroidal vs. cylindrical geometry effect. Except for the inertial effect, which distinguishes electric from magnetic elements, holding p fixed, an accelerator magnet with field B_y could be replaced by an electric element of the same length, with central field $E_r = \beta c B_y$ and these field indices, without changing the performance of the accelerator. Comparing with Eq. (78) one sees that $\bar{R} = r_0/n$, or

$$n = \frac{r_0}{\bar{R}}. \quad (81)$$

To incorporate the inertial effect also, using Eqs. (59) and (73), one can define an effective focusing coefficient

$$\begin{aligned} K_1^{(E,\text{eff.})} &= -\frac{1}{\bar{R}r_0} + \frac{1}{r_0^2} \frac{r_0 e E_{\text{nom.}}}{\mathcal{E}} \left(\frac{2}{\beta^2} - 1 \right) \\ &= -\frac{1}{\bar{R}r_0} + \frac{1}{r_0^2} \left(1 + \frac{1}{\gamma^2} \right). \end{aligned} \quad (82)$$

The effect of being in an electric field proportional to $1/r$, rather than a uniform magnetic field, is that the parenthesized factor would be 1 for a uniform $n = 0$ magnet. For a less than fully relativistic particle in a weak-focusing, large \bar{R} field, this would be a significant alteration; for example it causes the horizontal tune to be $(1 + 1/\gamma^2)$ rather than 1. For the ‘‘strong focusing’’ we anticipate, r_0 will be much greater than \bar{R} and the second term of Eq. (82) will be small or even negligible. For preliminary design studies, especially for strong focusing with $n \gg 1$ and $\bar{R} \approx r_0/n \ll r_0$, it seems justified to simply neglect this inertial effect

Another error being made is that the electric field is being calculated in 2D, cylindrical geometry when, in fact, the electrodes are curved longitudinally as well as transversely.

6.2 Transfer Map Determination

We can now generalize Eqs. (4) to incorporate Eqs. (66) and (82)

$$x'' + (ik_x^{\text{cf}})^2 x - \frac{\Delta}{r_0} = 0, \quad \text{where} \quad (ik_x^{\text{cf}})^2 = -\frac{1}{Rr_0} + \frac{1}{r_0^2} \left(1 + \frac{1}{\gamma^2}\right), \quad (83)$$

$$y'' + k_y^{\text{cf}2} y = 0, \quad \text{where} \quad k_y^{\text{cf}2} = \frac{1}{Rr_0}. \quad (84)$$

The longitudinal rigidity offset parameter Δ was defined in Eq. (67). Equations that are very nearly equivalent to these are derived in the Wollnik book[8]. The very different notation, especially concerning the definition of Δ , plus several minor misprints, makes it quite difficult to compare the formulas in detail however. Here we are following Wollnik's section 4.3.2[8], though varying his notation somewhat.

Intending to apply these formulas only to strongly horizontal defocusing elements, an explicit factor of i has been introduced so that we can assume that k_x^{cf} and k_y^{cf} are both real and positive. The general solutions of Eqs. (83) are

$$\begin{aligned} x(z) &= c_1 \cos ik_x^{\text{cf}} z - id_1 \sin ik_x^{\text{cf}} z - \frac{\Delta}{k_x^{\text{cf}2} r_0} \\ &= c_1 \cosh k_x^{\text{cf}} z + d_1 \sinh k_x^{\text{cf}} z - \frac{\Delta}{k_x^{\text{cf}2} r_0}, \end{aligned} \quad (85)$$

$$y(z) = c_2 \cos k_y^{\text{cf}} z + d_2 \sin k_y^{\text{cf}} z. \quad (86)$$

Eliminating c_1, d_1, c_2, d_2 , in favor of initial conditions $x_0, x'_0, \Delta_0, y_0, y'_0$, at $z = 0$, one obtains

$$\begin{pmatrix} x \\ x' \\ \Delta \end{pmatrix} = \begin{pmatrix} c_x & s_x & d_x \\ s_x k_x^{\text{cf}2} & c_x & s_x/r_0 \\ 0 & 0 & 1 \end{pmatrix} \begin{pmatrix} x_0 \\ x'_0 \\ \Delta_0 \end{pmatrix}, \quad (87)$$

$$\begin{pmatrix} y \\ y' \end{pmatrix} = \begin{pmatrix} c_y & s_y \\ -s_y k_y^{\text{cf}2} & c_y \end{pmatrix} \begin{pmatrix} y_0 \\ y'_0 \end{pmatrix}, \quad (88)$$

where

$$\begin{aligned} c_x &= \cosh k_x^{\text{cf}} z, & s_x &= \frac{\sinh k_x^{\text{cf}} z}{k_x^{\text{cf}}}, & d_x &= \frac{\cosh k_x^{\text{cf}} z - 1}{r_0 k_x^{\text{cf}2}}, \\ c_y &= \cos k_y^{\text{cf}} z, & s_y &= \frac{\sin k_y^{\text{cf}} z}{k_y^{\text{cf}}}. \end{aligned} \quad (89)$$

For small z the 1,2 elements reduce to the immediate drift length z and the 2, 1 components reduce to the inverse focal length ascribable to length z .

7 Space Charge Issues

7.1 Introduction

Estimates of the quantities discussed in this section have already been given by Alexei Fedotov[3]. I have tried to roughly match the bunch pattern and intensities that he introduced. (After fixing errors he pointed out) there is substantial agreement with his results. The presentation here (as elsewhere) is pretty long-winded, with formulas derived from scratch, largely for pedagogic purposes. Parameters are given in Table 2.

Table 1: Storage ring parameters

quantity	symbol	unit	low intensity	high intensity
protons per bunch	N_p		2.0e8	1.0e9
bunches per ring	N_B		24	24
instrumented IP's	$N_{instr.}$		16	16
instr. IP betas	β_x/β_y	m	0.1/0.1	0.1/0.1
no-instr. IP's			32	32
no-instr. IP betas	β_x/β_y	m	15/20	15/20
bunch length	σ_z	m	0.1	0.2
beam-beam tune shift	ξ		1.6e-3	0.8e-2
Laslett tune shift	$< \Delta Q_{Laslett} >$		0.036	0.090
p-p collision rate		1/s	1.6	39

7.2 Beam-Beam Tune Shift

The electric field at radius r in a round, transversely Gaussian (s.d. $\sigma_x = \sigma_y = \sigma$), cylindrical beam of line charge density $\lambda(z)$ is given by

$$\begin{pmatrix} E_x \\ E_y \end{pmatrix} = \frac{\lambda(z)}{2\pi\epsilon_0} \frac{1 - \exp(-r^2/(2\sigma^2))}{r^2} \begin{pmatrix} x \\ y \end{pmatrix} \approx \frac{\lambda(z)}{4\pi\epsilon_0\sigma^2} \begin{pmatrix} x \\ y \end{pmatrix}. \quad (90)$$

where the final, linearized, version is valid only near the beam axis. The magnetic fields are $B_x = \beta E_y/c$ and $B_y = -\beta E_x/c$, possibly with reversed signs, depending on the beam direction. In passing a distance Δz along the length of a single oncoming beam bunch, a counter-circulating proton suffers a (linearized) deflection

$$\begin{aligned} \Delta\theta_{x,1} \equiv x\Delta q_x &= \frac{\Delta p_x}{p_0} = \frac{e}{\beta\gamma m_p c^2} \frac{1}{4\pi\epsilon_0\sigma^2} (1 + \beta^2) \frac{\Delta z}{2\beta} \lambda(z) x \\ &= \frac{1}{2\beta^2\gamma} \frac{r_p}{\sigma^2} (1 + \beta^2) N_p P(z) \Delta z x, \end{aligned} \quad (91)$$

where $N_p P(z) \Delta z$ is the number of protons in the range Δz in a single bunch. For a longitudinally Gaussian bunch $P = \exp(-z^2/2\sigma_z^2)/\sqrt{2\pi\sigma_z^2}$. The first term

here is due to the electric field. The second is due to the magnetic field. The denominator factor 2β comes from the relative velocity $2v$. $r_p = e^2/(4\pi\epsilon_0 m_p c^2) = (0.511/938) \times 2.82 \times 10^{-15} = 1.54 \times 10^{-18}$ m is the classical proton radius.

This x -proportional deflection focuses (actually defocuses) the beam. By the ‘‘golden rule’’ for accelerator lattices, the focusing causes tune shift

$$\Delta Q_x = -\frac{1}{4\pi} \beta_x \Delta q_x. \quad (92)$$

(One must not confuse (horizontal) lattice function β_x and relativistic speed factor β .) Combining factors and integrating over z yields the tune shift caused by passage through a single oncoming bunch.

For non-round beams the calculation is more complicated. Skipping that discussion, combining factors and summing over $N_{\text{instr.}}$ bunch passages per turn, the summed beam-beam tune shift parameters with $N_{\text{instr.}}/2$ bunches in each beam are given by

$$\xi_{x,y} \equiv \Delta Q_{x,y} = -N_{\text{instr.}} N_p \frac{r_p}{\beta^2 \gamma} (1 + \beta^2) \frac{\beta_{x,y}^*/(4\pi)}{\sigma_x^* \sigma_{x,y}^* (1 + R)}, \quad (93)$$

where R , the beam aspect ratio at the IP, is defined by

$$R = \frac{\sigma_y^*}{\sigma_x^*}, \quad (94)$$

Assuming round beams ($R=1$) and unnormalized emittance $\epsilon = \sigma^2/\beta$, and substituting into Eq. (93),

$$\begin{aligned} \xi &= -N_{\text{instr.}} N_p \frac{r_p}{\beta^2 \gamma} (1 + \beta^2) \frac{\beta_{x,y}^*/(4\pi)}{\sigma_x^* \sigma_{x,y}^* (1 + R)} \\ &= -N_{\text{instr.}} N_p \frac{r_p}{\beta^2 \gamma} (1 + \beta^2) \frac{1}{8\pi\epsilon} \\ &= -(2 \times 24)(2 \times 10^8) \frac{1.54 \times 10^{-18}}{0.6^2 \times 1.25} \frac{1 + 0.6^2}{8\pi(6.7 \times 10^{-6}/6)} \\ &= 1.6 \times 10^{-3}. \end{aligned} \quad (95)$$

Beam-beam tune shifts greater than this are routinely achieved in existing storage rings.

7.3 Space Charge (Laslett) Tune Shift

Though a proton feels the force of protons in the counter-rotating beam only $N_{\text{instr.}}$ times per turn, it feels the force of protons in its own bunch all the time. One reason the tune shift calculation was spelled out in some detail in the previous section, was so that an intermediate result could be used here. Again the leading effect is a defocusing deflection that can be obtained by adapting Eq. (91);

$$\Delta\theta_{x,1} \equiv x\Delta q_x = \frac{1}{\beta^2 \gamma^3} \frac{r_p}{\sigma^2} N_p P(z) \Delta z x, \quad (96)$$

The sign of the magnetic deflection has been reversed, and $1 - \beta^2 = 1/\gamma^2$. Δz is now to be interpreted as an increment of longitudinal distance along the ring, and the relative speed is now v rather than $2v$. Copying from Eq. (93), the tune shift of a particle traveling one turn around the machine at position z in a bunch is

$$\Delta Q_{\text{Laslett}}(z) = -N_p P(z) \mathcal{C}_0 \frac{r_p}{\beta^2 \gamma^3} \frac{1}{4\pi\epsilon}, \quad (97)$$

where \mathcal{C}_0 is the lattice circumference. The average over positions z of $P(z)$ is

$$\langle P(z) \rangle = \int_{-\infty}^{\infty} P^2(z) dz = \frac{1}{2\pi\sigma_z^2} \int_{-\infty}^{\infty} e^{-z^2/\sigma_z^2} dz = \frac{1}{2\sqrt{\pi}\sigma_z}. \quad (98)$$

Substituting into Eq. (97) yields

$$\begin{aligned} \langle \Delta Q_{\text{Laslett}} \rangle &= -N_p \frac{r_p}{\beta^2 \gamma^3} \frac{1}{8\pi^{3/2}\epsilon} \frac{\mathcal{C}_0}{\sigma_z} \\ &= -(2 \times 10^8) \frac{1.54 \times 10^{-18}}{(0.6^2)(1.25^3)} \frac{1}{8\pi^{(3/2)}(6.7 \times 10^{-6}/6)} \frac{\mathcal{C}_0}{\sigma_z} \\ &= 0.881 \times 10^{-5} \frac{\mathcal{C}_0}{\sigma_z} \quad \left(\text{e.g. } (0.881 \times 10^{-5}) \frac{414}{0.1} = 0.036 \right). \end{aligned} \quad (99)$$

This value of $\langle \Delta Q_{\text{Laslett}} \rangle$ seems acceptably small.

Fedotov[4] gives a generalized version of this formula that is applicable to non-round beams;

$$\Delta Q_{x,y} = -\frac{N_p r_p}{2^{3/2} \pi^{3/2} \beta^2 \gamma^3} \frac{1}{\epsilon_{x,y} \left(1 + \sqrt{\frac{\epsilon_{y,x} Q_x}{\epsilon_{x,y} Q_y}} \right)} \frac{\mathcal{C}_0}{\sigma_z} \quad (100)$$

Fedotov's calculated tune shifts are $Q_x = 0.012$ and $Q_y = 0.007$, both smaller than the value 0.036 calculated in Eq. (99). The difference is primarily due to his smaller assumed circumference (212/414) and larger bunch length (0.4/0.1).

For round beams Eq. (100) agrees with Eq. (99) (except for a factor $\sqrt{2}$). This factor may correspond to a different averaging of the tune shift. In any case the tune shift is necessarily somewhat vague since, because different particles take up longitudinal positions z with different probabilities, they suffer different tune shifts. In any case the discrepancy is small enough to ignore for the present purposes.

Experimental data giving limiting values of Laslett tune shift at our (quite low) beam energy are largely obtained during injection into higher energy accelerators. Since the beams remain at low energy only briefly the limits directly apply limits on the long term stability of the EDM storage rings. With this reservation, Machida[5] calculations show little transverse beam blow-up for tune shifts below 0.25. Weng[6] gives tune shifts in excess of 0.30 in the AGS during injection of 2×10^{13} protons of 200 MeV kinetic energy.

7.4 Luminosity

Tentative collision point optics have been shown in Fig. ?? or Fig. ?. The crossing point beta function values are $\beta_x^* = \beta_y^* = 0.1$ m. Following Sands[10], the luminosity \mathcal{L}_1 at one collision point in a collider is given by

$$\mathcal{L}_1 = \frac{f}{4} \frac{N_p^2}{A_{\text{int}}} \quad (101)$$

where N_p is the number of protons in each bunch. The revolution frequency is $f = 3 \times 10^8 / 413.6 = 0.72$ MHz. A_{int} is an effective interaction area. This formula assumes there is a single bunch in each beam. Summing the luminosities from all collision points yields

$$\mathcal{L}_{\text{sum}} = N_{\text{instr.}} \frac{f}{4} \frac{N_p^2}{A_{\text{int}}} \quad (102)$$

where $N_{\text{instr.}}$ is the number of instrumented low beta intersection points. As such it is double the number of “effective” bunches whose p-p scatters and asymmetries can be counted. All these collision points are assumed to be identical.

The reason for introducing effective bunches is that some of the bunch crossings may occur at non-waist, not-very-low- β lattice points. Not only will the collision rates at these points be very small, what there are will not be counted. Our example has $N_{\text{instr.}} = 16$ low beta intersection points but 24 stored bunches. Of the 48 collision points, the only appreciable p-p scatters occur at the 16 instrumented IP’s.

Alexei Fedotov[3] has given $\epsilon_{n,95} = 5 \mu\text{m}$ as a tentative normalized emittance containing 95% of the particles. With $\beta = 0.60$ and $\gamma = 1.25$, this corresponds to “geometric” emittance $\epsilon_{95} = \epsilon_{n,95} / (\beta\gamma) = 6.7 \mu\text{m}$. Fedotov also states that 95% emittances and r.m.s. emittances are related by $\epsilon_{95} = 6\epsilon \equiv 6\sigma^2 / \beta$. At the collision point, with $\beta_x = \beta_y = \beta^*$, the beam standard deviations are

$$\sigma^* \approx \sqrt{\beta^* \epsilon_{95} / 6} \quad \left(\text{e.g.} \sqrt{0.1 \times 6.7 \times 10^{-6} / 6} = 0.334 \text{ mm} \right). \quad (103)$$

With head-on collisions of short bunches³ the effective crossing area is the same as the bunch transverse area, which Sands[10], Eq. (6.2) gives as

$$A_{\text{int}} \approx \pi \sigma_x \sigma_y \quad \left(\text{e.g.} \ 0.0334^2 \pi = 3.5 \times 10^{-3} \text{ cm}^2 \right). \quad (104)$$

Here we assume $N_p = 10^9$. Combining factors one obtains, for the summed luminosity,

$$\mathcal{L}_{\text{sum}} \approx N_{\text{instr.}} \frac{f}{4} \frac{N_p^2}{A_{\text{int}}} \quad \left(\text{e.g.} \ 16 \frac{0.72 \times 10^6}{4} \frac{10^{18}}{3.5 \times 10^{-3}} = 0.82 \times 10^{27} \text{ cm}^{-2} \text{ s}^{-1} \right). \quad (105)$$

³“Short” bunches are short compared to the beta functions at the crossing point. In the proton EDM experiment the bunches may be too long to meet this condition. This would reduce the luminosity, but we will ignore this complication.

Here $N_{\text{instr.}} = 16$ bunch crossings have been assumed, and the luminosity is quoted in its customary c.g.s. units. It is roughly one inverse millibarn per second.

7.5 p-p Collision Rates

Some circulating beam kinematic quantities are

$\gamma_0 = 1.24810$
 $E_0 = 1.17106 \text{ GeV}$
 $K_0 = 0.23279 \text{ GeV}$
 $p_0c = 0.700740 \text{ GeV}$
 $\beta_0 = 0.598379$
 $\eta_0 = 0.12405$

For p-p collisions, the square of the center of mass energy is

$$s = 4 E_0^2 = 5.485568860 \text{ GeV}^2$$

To achieve this value with one proton being at rest in the laboratory requires the laboratory energy of the other proton to be

$$E_{\text{lab.}} = \frac{s - 2(mc^2)^2}{2mc^2} \quad (106)$$

Then

$E_{\text{lab}} = 1.98495 \text{ GeV}$
 $K_{\text{lab}} = 1.04668 \text{ GeV}$
 $p_{\text{lab}} = 1.73256 \text{ GeV}$

From Bugg et al.[11] the total inelastic p-p cross sections at this energy is $\sigma_{\text{tot.}} = 48 \text{ mb}$ and the total elastic cross section is $\sigma_{\text{elastic}} = 23 \text{ mb}$. Multiplying the total cross section by the luminosity one obtains the scattering rate

$$\rho_{\text{tot.}} = (0.82 \times 10^{27}) \times (48 \times 10^{-27}) = 39 \text{ scatters per second}, \quad (107)$$

of which half are elastic. This rate is discouragingly small, in spite of having increased the proton intensity to its largest plausible value, and having reduced β^* to the smallest value consistent with electrostatic focusing.⁴ This rate corresponds to a beam lifetime of

$$\tau = \frac{N_p N_B}{\rho_{\text{tot.}}} = \frac{10^9 \times 24}{39} \approx 6 \times 10^8 \text{ s}, \quad (108)$$

which is far longer than the anticipated useful storage time of 10^3 seconds. Actual beam loss from this source is therefore negligible. But it will be seen below that the scattering asymmetry (for optimal spin configuration) is so large that a meaningful polarization measurement can be obtained in a few seconds.

⁴With magnetic focusing smaller values of β^* could be achieved, but that option has been ruled out, at least for this report. The rate *could* be almost tripled by designing a lattice with all collision points having low beta values. But this would force the circumference to be appreciably greater. The presently assumed circumference value, $C_0 = 416 \text{ m}$, has already been substantially lengthened by its 16 IP requirement.

8 Synchrotron Oscillations and Spin Precession

The averaging effect of synchrotron oscillations is essential for achieving the long spin decoherence times essential for the proton EDM experiment. The angular precession rate of a proton depends on the local \mathbf{B} or \mathbf{E} field, and on its velocity (or momentum, or energy or β or γ). The deviation of the spin precession rate from the momentum precession rate is the difference of two terms that cancel in the “magic” condition. To lowest order in deviation from magic, it does not matter which of the dynamic quantities is chosen as dependent variable.

The RF cavity applies an impulsive boost to the particle’s energy \mathcal{E} . This makes it natural to use $\gamma = \mathcal{E}/(m_p c^2)$ as the dependent synchrotron oscillation variable, along with time t or turn index j as the independent variable. From $\gamma(t)$ so obtained, and the field values encountered on its orbit, one can calculate the spin precession of any particular proton.

The magic condition for the spin precession rate to match the momentum precession rate can be expressed as

$$\gamma_0 = \sqrt{\frac{g}{g-2}} = \sqrt{\frac{5.5856}{3.5856}} = 1.248. \quad (109)$$

We will express the precise γ value of a particular proton as

$$\gamma_j = \gamma_0 + \Delta\gamma_j + \delta\gamma_0, \quad (110)$$

where $\Delta\gamma_j$ is the synchrotron oscillation part, which varies with turn number j and $\delta\gamma_0$ will later be split into two parts, $\delta\gamma_{0,1}$ a deviation from the magic value due to the fact that the average beam energy is not quite correct, and $\delta\gamma_{0,2}$ is due to the proton’s betatron amplitude. For the time being we assume $\delta\gamma_0 = 0$, meaning that any effect of betatron oscillations is being neglected and the average energies of both counter-circulating beams have been exactly matched to the ideal value.

With the RF frequency fixed, the flight time of a proton in a stable bucket increases, on average, by $T_0 = 2\pi h/\omega_{\text{RF}}$ each turn. This average can be taken to be arbitrarily accurate over the enormous number of turns during which parameters are typically held fixed. But the paths taken by different particles are different and their average instantaneous speeds are therefore different. As a result their spin vectors precess at different rates.

An inconvenience to be faced is that the treatment of synchrotron oscillations has to be different in magnetostatic and electrostatic rings. In the arcs of a magnetic lattice, though γ changes discontinuously in the RF cavity, it is constant in the arcs. In an electric bending element the proton energy changes with changing radial position.

8.1 Averaging Over Energy

With synchrotron oscillations so well understood, it may seem gratuitous to derive their properties as will be done next. The justification is to exercise

tools, elementary but somewhat unconventional, that will be used to analyse spin precession in the following subsection.

Let $T(\gamma)$ be the revolution period as a function of $\gamma = \gamma_0 + \Delta\gamma$, and let $j = 0, 1, 2, \dots$ be a turn counter that augments by 1 on each passage through a fixed point in the lattice, conveniently taken to be at the center of the (single) RF cavity. The arrival times (relative to reference) are then t_0, t_1, t_2, \dots . Let $\Delta\gamma_{j+}$ be the γ -deviation during the full turn from j to $j + 1$ and $\Delta\gamma_{j-}$ be the deviation during the preceding turn. (For off-momentum particles in an electrostatic ring γ is not quite a constant of the motion. But γ is constant for the design (reference) particle. For off-momentum particles in electric lattices γ will stand for the energy *outside* electric fields.)

With $t_{j+1} - t_j = T(\gamma_0 + \Delta\gamma_{j+})$, and a similar equation for t_{j-1} , the arrival times satisfy the difference equation

$$\begin{aligned} t_{j+1} - 2t_j + t_{j-1} &= T(\gamma_0 + \Delta\gamma_{j+}) - T(\gamma_0 + \Delta\gamma_{j-}) \\ &= \left. \frac{\partial T}{\partial \gamma} \right|_0 (\Delta\gamma_{j+} - \Delta\gamma_{j-}) + \frac{1}{2} \left. \frac{\partial^2 T}{\partial \gamma^2} \right|_0 (\Delta\gamma_{j+}^2 - \Delta\gamma_{j-}^2) + \dots \end{aligned} \quad (111)$$

To make the quadratic term vanish we assume the lattice has been designed so that

$$\left. \frac{\partial^2 T}{\partial \gamma^2} \right|_0 = 0, \quad (112)$$

and we assume that all subsequent terms are negligible. In other words, we assume the graph of $T(\gamma)$ is a perfect straight line for the full range of γ values in the beam.⁵ (Remember, also, that betatron amplitudes have been set to zero.)

A task for the lattice designer is to meet this requirement. The following digression shows that the condition can be met, at least in special cases.

Digression:

(a) Weak Focusing, Magnetic Lattice. In a weak focusing magnetic lattice the central radius r_0 and the magnetic field $B(r)$ are independent of the longitudinal coordinate. The revolution period T can be obtained from

$$r = \frac{m_p v \gamma}{e B(\gamma)} \stackrel{\text{also}}{=} \frac{v T}{2\pi}, \quad \text{giving} \quad T = \frac{2\pi m_p}{e} \frac{\gamma}{B(\gamma)}. \quad (113)$$

(All of the quantities r , T , and B , depend on γ , but the dependence has only been shown for $B(\gamma)$, as we wish to tailor the radial dependence of B .) Solving differential equation (112), one finds

$$B(\gamma) = \frac{B_0}{B_0 c_2 + (1 - B_0 c_2) \gamma_0 / \gamma}, \quad (114)$$

⁵Though the discussion has not been formulated in terms of field multipoles, condition (112) implies the existence of sextupole fields superimposed on the combined function elements, as well as actual sextupoles.

where the integration constants have been chosen so that $B = B_0$ when $\gamma = \gamma_0$, and c_2 is a free parameter. The effect of the RF is to enforce $T = T_0$, which can be manipulated to produce

$$\frac{1}{\gamma} = \sqrt{1 - \left(\frac{2\pi r}{cT_0}\right)^2}, \quad \text{and} \quad B(\gamma) = \frac{B_0}{B_0 c_2 + (1 - B_0 c_2) \gamma_0 \sqrt{1 - \left(\frac{2\pi r}{cT_0}\right)^2}}. \quad (115)$$

(b) Weak Focusing, Electric Lattice.

In an electric lattice Eq. (113) is altered to

$$r = \frac{m_p \tilde{v}^2 \tilde{\gamma}}{eE(\gamma)} \stackrel{\text{also}}{=} \frac{\tilde{v}T}{2\pi}, \quad (116)$$

where

$$\tilde{\gamma} = \gamma + \frac{eE_0}{m_p c^2} (r - r_0), \quad \text{and} \quad \tilde{v}^2 = c^2 \left(1 - \frac{1}{\tilde{\gamma}^2}\right) \quad (117)$$

allow for the altered particle energy as a function of radial position in the electric bending field. Note that E_0 is negative. Also, in spite of the fact that the proton is inside the bending field essentially all the time, γ continues to stand for the value the proton would have outside, for example at the center of the RF cavity. Obtaining T as a function of γ is more complicated in this case, which further complicates, but is unlikely to prevent, obtaining the dependence of E on r needed to satisfy Eq. (112).

End of Digression.

The effect of the RF cavity is to alter the particle energy according to

$$\Delta\gamma_{j+} - \Delta\gamma_{j-} = -\frac{e\hat{V}_{RF}}{m_p c^2} \sin(\omega_{RF}(jT_0 + t_j)) = -\frac{e\hat{V}_{RF}}{m_p c^2} \sin(\omega_{RF}t_j), \quad (118)$$

where T_0 is the design revolution period, $\omega_{RF} = 2\pi h/T_0$, integer h is called the harmonic number, and the time origin has been adjusted so that the RF voltage vanishes at $t = 0$. For small time deviations from 0,

$$V_{RF}(t) \approx \hat{V}_{RF} \omega_{RF} t. \quad (119)$$

Substitution into Eq. (111) yields

$$t_{j+1} - 2t_j + t_{j-1} = -\frac{\partial T}{\partial \gamma} \Big|_0 \frac{e\hat{V}_{RF}}{m_p c^2} \sin(\omega_{RF,0}t_j). \quad (120)$$

The linearized (small t_j) version of this equation is

$$t_{j+1} - 2\cos\mu_s t_j + t_{j-1} = 0, \quad (121)$$

where⁶

$$\cos\mu_s = 1 - \frac{1}{2} \frac{dT}{d\gamma} \Big|_0 \frac{e\hat{V}_{RF}}{m_p c^2} \omega_{RF}; \quad (122)$$

⁶Note that \hat{V}_{RF} is not necessarily positive, but the product $\hat{V}_{RF} dT/d\gamma$ has to be positive for $\cos\mu_s$ to correspond to a real angle μ_s .

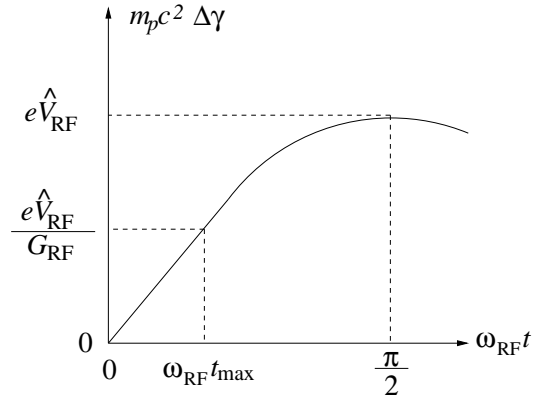


Figure 6: RF waveform and definition of overvoltage factor G_{RF} ; $\sin(\omega_{RF} t_{\max}) = 1/G_{RF}$. For $G_{RF} > \sim 2$, $t_{\max} \approx 1/(G_{RF} \omega_{RF})$. Because the operating point is at the origin, there is faithful averaging even for particle amplitudes large enough for the motion to be nonlinear.

The general solution of this linearized equation is

$$t_j = t_{\max} \sin(\mu_s j + \phi_0). \quad (123)$$

t_{\max} and ϕ_0 are fixed by the initial conditions for a particular proton being tracked, $t_0 = t_{\max} \sin \phi_0$. (In the next subsection, where spin direction evolution is analysed, the spin direction at this instant will be taken to be α_0 .) For the evolution of $\Delta\gamma_j$ we try

$$\Delta\gamma_j = -\Delta\gamma_{\max} \cos(\mu_s j + \phi_0). \quad (124)$$

The change in $\Delta\gamma_j$ in one turn then has to be

$$\begin{aligned} \frac{d}{dj} \Delta\gamma_j &= \Delta\gamma_{\max} \mu_s \sin(\mu_s j + \phi_0) \\ &\stackrel{\text{also}}{=} \frac{e \hat{V}_{RF}}{m_p c^2} \sin(\omega_{RF} t_j) \\ &= \frac{e \hat{V}_{RF}}{m_p c^2} \omega_{RF} t_{\max} \sin(\mu_s j + \phi_0), \end{aligned} \quad (125)$$

where t_j , as given by Eq. (123), has been assumed to be small. The maximum time and energy excursions are then related by

$$\Delta\gamma_{\max} = \frac{e \hat{V}_{RF}}{m_p c^2} \frac{\omega_{RF}}{\mu_s} t_{\max}. \quad (126)$$

The maximum γ change per turn $(d\Delta\gamma/dj)_{\max}$ can also be expressed in terms of the ‘‘overvoltage factor’’ G_{RF} shown in Fig. 6, and as the coefficient of the

first of Eqs.(125);

$$\left. \frac{d\Delta\gamma}{dj} \right|_{\max} = \frac{1}{G_{RF}} \frac{e\hat{V}_{RF}}{m_p c^2} = \mu_s \Delta\gamma_{\max}. \quad (127)$$

So $\Delta\gamma_{\max}$ is also given by

$$\Delta\gamma_{\max} = \frac{1}{G_{RF}} \frac{e\hat{V}_{RF}}{m_p c^2} \frac{1}{\mu_s}. \quad (128)$$

From Eq. (126) we then also have

$$t_{\max} \approx \frac{1}{\omega_{RF}} \frac{1}{G_{RF}}. \quad (129)$$

This equation is expressed only as an approximation since it manifestly disagrees with the definition of G_{RF} shown in Fig. 6. The disagreement has come from the linearization assumptions. For $G_{RF} > 2$ the disagreement is less than 5%.

This is pure (digital) simple harmonic motion and $\Delta\gamma_j$ averages exactly to zero over many turns. Furthermore the symmetry of the equations is such that this averaging to zero will apply even when the linearization ceases to be a good approximation.

One may say that this is no surprise—we knew all along, from established theory that $\Delta\gamma_j$ had to average to zero. But before McMillan and Veksler invented synchrotron stability, they did not know that $\Delta\gamma_j$ had to average to zero. For that matter, had we started with energy offset $\delta\gamma_0 \neq 0$, then $\Delta\gamma_j$ would have had to average to $-\delta\gamma_0$ divided by the number of terms in the average. Or, if the RF phase were varied monotonically, the proton could actually be systematically accelerated. All that has been shown, then, is that the formulas introduced so far conform with well established accelerator physics.

So far these comments have applied just to the linearized longitudinal equation of motion. But, if the graph of $T(\gamma)$ is a perfect straight line for the full range of γ values in the beam, and the design orbit is matched to the magic value γ_0 , then, averaging over many turns,

$$\langle \gamma_j \rangle = \gamma_0, \quad (130)$$

even for large momentum offsets (though small enough for the proton to stay in its stable bucket).

In a purely magnetic lattice γ is a constant of the motion. A particle having always the “magic” γ would behave like a Dirac particle. That is, its spin would exactly track its momentum, irrespective of its betatron oscillation amplitudes. This seems to make the averaging principle quite powerful, at least in magnetic lattices. But betatron oscillations cause the magic condition to be not satisfied on an instantaneous basis, which weakens the effectiveness of the averaging. (In practice the magic condition will also be not quite satisfied because of not quite correct beam energy, but ways of cancelling this drift over time are easily imagined.)

In an electrostatic lattice, γ is *not* a constant of the motion. One can hope, however, that the shifts due to radial energy changes will average out to adequate accuracy.

8.2 Spin Precession

Still neglecting the effect of betatron oscillations, it will be shown that the spin orientation angle of an individual proton can be expressed as the sum of the following four terms:

$$\alpha_j = \alpha_0 + 2\pi \left(\frac{g}{2} - 1 + \frac{g/2}{\gamma_0^2} \right) \delta\gamma_0 j + \alpha_j^{(F)} + \alpha_j^{(N)}. \quad (131)$$

The first is an initial condition, the second is due to mean energy deviation (which is correctable, on the average, over time) and (only partially correctable) effects of betatron oscillation, the third is fast oscillation synchronized with longitudinal oscillations, and the fourth is (probably negligible) resonant depolarization. Assuming the polarization orientation can be monitored and fed back via the RF frequency, the dominant limitation for the proton EDM experiment will be spin depolarization due to betatron oscillations.

The synchrotron tune Q_s only needs to be high enough to limit the sweeping action of the $\alpha_j^{(F)}$ term to an acceptably small angular range, such as $\pm 0.5 r$.

8.2.1 Small Amplitudes, No Deviation from “Magic” Condition

We remind again that betatron oscillations have been, and will, in this subsection, continue to be, neglected. That is we assume all betatron amplitudes are small enough to have no effect on the revolution period. We also assume the central beam energy is exactly matched to the magic value.

The leading impediment to measurement of the proton electric dipole moment (other than its smallness) is the precession of the proton axis due to its magnetic moment. With the spin vector \mathbf{s} starting in the forward direction, and the magnetic field (in the proton rest frame) vertical, \mathbf{s} remains in the horizontal plane. See Fig. 7. Jackson’s[9] Eq. (11.171) gives the rate of change in an electric field \mathbf{E} , of the longitudinal spin component as

$$\frac{d}{dt} (\hat{\beta} \cdot \mathbf{s}) = -\frac{e}{m_p c} \mathbf{s}_\perp \cdot \mathbf{E} \left(\frac{g\beta}{2} - \frac{1}{\beta} \right) \quad (132)$$

Using $\hat{\beta} \cdot \mathbf{s} = s \cos \alpha$, $\mathbf{s}_\perp = -\hat{\mathbf{x}} s \sin \alpha$, and $\mathbf{E} = -\hat{\mathbf{x}} E$, this equation reduces to

$$\frac{d\alpha}{dt} = \frac{eE}{m_p c} \left(\frac{g\beta}{2} - \frac{1}{\beta} \right). \quad (133)$$

Meanwhile the velocity vector itself has precessed by angle θ relative to a direction fixed in the laboratory. Its precession rate is governed by the equation

$$\frac{d\theta}{dt} = \frac{d}{dt} \left(\frac{s}{r} \right) = \frac{eE}{p}. \quad (134)$$

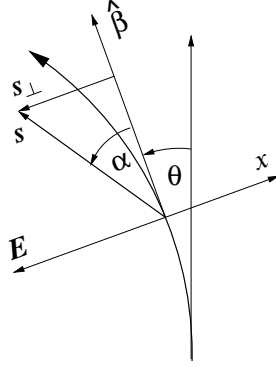


Figure 7: Spin vector \mathbf{s} has precessed through angle α away from its nominal direction along the proton's velocity.

where, as in Eq. (59), the curvature is $1/r = eE/(vp)$ and where (just in this equation) s temporarily stands for arc length along the orbit. Dividing Eq. (133) by Eq. (134) yields

$$\frac{d\alpha}{d\theta} = \frac{pc}{m_p c^2} \left(\frac{g\beta}{2} - \frac{1}{\beta} \right) = \left(\frac{g}{2} - 1 \right) \gamma - \frac{g/2}{\gamma}. \quad (135)$$

One can check that $d\alpha/d\theta$ vanishes at the magic condition $\gamma = \gamma_0$. During a single turn around the ring θ advances by 2π and the advance of α can be obtained from this equation. Introducing $\gamma_{j\pm} = \gamma_0 + \Delta\gamma_{j\pm}$ as in Section 8.1, α_j satisfies the difference equations

$$\begin{aligned} \alpha_{j+1} - \alpha_j &= 2\pi \left(\frac{g-2}{2} \gamma_{j+} - \frac{g/2}{\gamma_{j+}} \right), \\ \alpha_j - \alpha_{j-1} &= 2\pi \left(\frac{g-2}{2} \gamma_{j-} - \frac{g/2}{\gamma_{j-}} \right). \end{aligned} \quad (136)$$

Subtracting these equations yields

$$\begin{aligned} \alpha_{j+1} - 2\alpha_j + \alpha_{j-1} &= 2\pi \left(\frac{g-2}{2} (\gamma_{j+} - \gamma_{j-}) - \frac{g}{2} \left(\frac{1}{\gamma_{j+}} - \frac{1}{\gamma_{j-}} \right) \right) \\ &\approx 2\pi \left(\frac{g-2}{2} + \frac{g/2}{\gamma_j^2} \right) (\Delta\gamma_{j+} - \Delta\gamma_{j-}), \end{aligned} \quad (137)$$

where Eqs. (118) has been used. The motivation for these manipulations has been to introduce and replace the common factor $(\Delta\gamma_{j+} - \Delta\gamma_{j-})$ that plays a prominent role in the description of the synchrotron oscillations themselves.

Substitution from Eqs. (118), (123), and (126), and assuming small t_j yields

$$\begin{aligned}
& \alpha_{j+1} - 2\alpha_j + \alpha_{j-1} \\
&= -2\pi \left(\frac{g-2}{2} + \frac{g/2}{\gamma_j^2} \right) \left(\frac{e\hat{V}_{RF}}{m_p c^2} \sin(\omega_{RF} t_j) \right) \\
&= -2\pi \left(\frac{g-2}{2} + \frac{g/2}{\gamma_j^2} \right) \mu_s \Delta\gamma_{\max} \sin(\mu_s j + \phi_0). \tag{138}
\end{aligned}$$

From here on we set $\phi_0 = 0$.

The only significant approximation that has been made so far has been the replacement of the product $\gamma_{j+}\gamma_{j-}$ by γ_j^2 in the denominator of the second term of the parenthesized factor. The average error from this replacement is

$$\langle \gamma_{j+}\gamma_{j-} \rangle - \gamma_j^2 = -\Delta\gamma_{\max}^2 \mu_s^2 / 8. \tag{139}$$

This seems certain to be negligible (especially because it only introduces a small fractional variation in the coefficient of the time-varying factor $\sin(\mu_s j)$).

We defer consideration of the nonlinear term $1/\gamma_j^2$ in Eq. (138) (which complicates the difference equation significantly) and approximate $\gamma_j \approx \gamma_0$. In this approximation the motion of α is governed by the discretized version of *driven* simple harmonic motion at frequency μ_s ;

$$\begin{aligned}
\alpha_j &= \alpha_0 + \pi \Delta\gamma_{\max} \mu_s \left(\frac{g-2}{2} + \frac{g/2}{\gamma_0^2} \right) \frac{\sin(\mu_s j)}{1 - \cos \mu_s} \\
&= \alpha_0 + 11.26 \Delta\gamma_{\max} \mu_s \frac{\sin(\mu_s j)}{1 - \cos \mu_s}. \tag{140}
\end{aligned}$$

where the initial spin direction is α_0 . Notice that the constant term α_0 satisfies the difference equation all by itself. For that matter a term $\alpha_j = \alpha'_0 j$ also satisfies the difference equation for arbitrary constant α'_0 . We neglect this possibility for now, but will return to it in Section 8.2.2. In this approximation there is “fast” synchrotron oscillation about α_0 . The amplitude of this fast oscillation is given by

$$\begin{aligned}
\alpha_{\max}^{(F)} &= \pi \Delta\gamma_{\max} \left(\frac{g-2}{2} + \frac{g/2}{\gamma_0^2} \right) \frac{\mu_s}{1 - \cos \mu_s} \\
&\approx \Delta\gamma_{\max} \left(\frac{g-2}{2} + \frac{g/2}{\gamma_0^2} \right) \frac{2\pi}{\mu_s} \\
&= 3.586 \frac{\Delta\gamma_{\max}}{Q_s}. \tag{141}
\end{aligned}$$

assuming $\mu_s \equiv 2\pi Q_s \ll 1$.

Consider next the effect of the $1/\gamma_j^2$ term in Eq. (118). The equation can be solved by first expanding $\sin(\mu_s j)/\gamma_j^2$ into a Fourier series, for example using the expansion

$$\frac{\sin \mu_s j}{(1 + a \cos \mu_s j)^2} - \sin(\mu_s j) = -a \sin(2\mu_s j) + \frac{3}{4} a^2 \sin(3\mu_s j) - \frac{1}{2} a^3 \sin(4\mu_s j) + \dots, \tag{142}$$

where, in each harmonic term, only the lowest power of

$$a = \frac{\Delta\gamma_{\max}}{\gamma_0} \quad (143)$$

has been retained. Two features of the Fourier series are especially noteworthy. It has no constant term and, with, presumably, $G_{RF}\Delta\gamma_{\max} \ll \gamma_0$, it is rapidly convergent. The drive term in Eq. (138) is now a sum of monochromatic terms, and the motion is the superposition of harmonic motions at the fundamental “frequency” μ_s and higher harmonic frequencies $j\mu_s$.

The response to the higher harmonic drive terms of Eq. (142) needs to be added to the linear motion of Eq. (140). The newly added nonlinear response terms are

$$\alpha_j^{(N)} = \pi\Delta\gamma_{\max}\mu_s \frac{g/2}{\gamma_0^2} \quad (144)$$

$$\times \left(-a \frac{\sin(2\mu_s j)}{1 - \cos 2\mu_s} + \frac{3}{4} a^2 \frac{\sin(3\mu_s j)}{1 - \cos 3\mu_s} - \frac{1}{2} a^3 \frac{\sin(4\mu_s j)}{1 - \cos 4\mu_s} + \dots \right).$$

There is now the possibility of resonance. This is most conveniently analysed in terms of the tune $Q_s = \mu_s/(2\pi)$, whose typical value is near the low end of the range $0 < Q_s < 1$. When $Q_s = l/m$, where l and m are integers, there is a term in the expansion for which $\cos(m\mu_s) = 1$. According to Eq. (144) this term exhibits uncontrollable secular growth.

The tune $Q_s = \mu_s/(2\pi)$ is sure to be much less than 1. The closest resonance is therefore at $Q_s = 0$. A constant term (i.e. independent of j) on the right hand side of Eq. (138) would drive this resonance. Fortunately, as noted previously, there is no constant term in Eq. (142). The beam polarization is therefore protected from at least this possible source of decoherence. (This is due, however to our assumption so far that the beam energy has exactly the magic value. The effect of deviation from this assumption is discussed in Section 8.2.2.)

No matter what the value of μ_s there will be values of l and m for which the resonance condition is approximately satisfied. In a real beam, with its continuum of synchrotron tunes (over finite time intervals), the resonance condition will be exactly satisfied for some particles over lengthy periods of time. Commonly in such situations, the effect of increased amplitude is to pull the frequency off resonance. But in our case, with Stern-Gerlach forces neglected, the secular growth of α has no effect whatsoever on the particle’s synchrotron tune. Clearly the fraction of the beam containing particles having tunes on resonance long enough will be depolarized.

Because $Q_s \ll 1$, resonance will occur only in very high order where the Fourier coefficients are very small. From what has been said, if the $Q_s = 0$ resonance is, in fact, unimportant, this suggests that *low* synchrotron tunes are advantageous. But Q_s has to be at least high enough to keep $\Delta\alpha_{\max} \ll \pi$. Otherwise the average up-down tipping of the proton axis caused by the electric dipole moment would be reduced unacceptably.

The $Q_s = 0$ resonance makes its presence known largely through the factor $1 - \cos \mu_s$ in the denominator of Eq. (141) which causes the angular amplitude

of spin oscillation per unit γ -deviation to be inversely proportional to Q_s , as shown in Eq. (141).

8.2.2 Deviant Beam Energy

To account for systematic deviation of $\delta\gamma_0$ of the central beam energy from the magic value γ_0 Eq. (135) can be expanded

$$\frac{d\alpha}{d\theta} = \left(\frac{g}{2} - 1\right) (\gamma_0 + \delta\gamma_0) - \frac{g/2}{\gamma_0 + \delta\gamma_0} = \left(\frac{g}{2} - 1 + \frac{g/2}{\gamma_0^2} + \dots\right) \delta\gamma_0. \quad (145)$$

Averaging this equation over multiple terms, and dropping higher order terms yields

$$\left\langle \frac{d\alpha}{d\theta} \right\rangle = \left(\frac{g}{2} - 1 + \frac{g/2}{\gamma_0^2}\right) \delta\gamma_0 = 3.586 \delta\gamma_0. \quad (146)$$

(There is no need to write $\langle \delta\gamma_0 \rangle$ since, as defined, $\delta\gamma_0$ already stands for that average.)

Spin evolution with $\delta\gamma_0 = 0$ has been described already by Eqs. (140), (141), and (144), which give α_j as the initial spin direction, $\alpha_j^{(F)}$ as fast, synchrotron oscillation induced oscillation, and $\alpha_j^{(N)}$ as oscillations at higher harmonics of the synchrotron frequency. None of these terms cause secular drift of the polarization axis, such as given by Eq. (146). Including the contribution from Eq. (146) yields

$$\alpha_j = \alpha_0 + 2\pi \left(\frac{g}{2} - 1 + \frac{g/2}{\gamma_0^2}\right) \delta\gamma_0 j + \alpha_j^{(F)} + \alpha_j^{(N)}. \quad (147)$$

It was already noted, below Eq. (140), that a term like this, linear in j , could be added without violating the difference equation.

One way or another, a way will have to be found to cancel the inexorable drift given by the second term. If the polarization vector orientation can be measured quickly enough (which seems likely) then the drift can be reversed and controlled.

9 Betatron-Induced Decoherence

The fact that we do not yet have a self-consistent formalism for electrostatic lattices is nowhere more important than in this section. Formulas applicable for magnetic lattices are used in conjunction with electrostatic formulas. Much of the discussion should not be affected qualitatively by this defect, but precession compensation formulas will, as a result, certainly not be quantitatively accurate. The presentation is intended, therefore, mainly as a template for subsequent, more realistic, calculations. To simplify the formulas weak focusing is mainly assumed.

For each injected proton, one assumes that unambiguous phase space amplitudes and phases, (a_x, ψ_x) , (a_y, ψ_y) , (a_s, ψ_s) , can be assigned. It can be noted

in passing that this is fully useful only in the absence of cross-plane correlation in six dimensions. Stated differently, it is assumed that the injected beam is matched perfectly to the lattice upon injection. Otherwise filamentation will inevitably lead to emittance growth (and possibly to some immediate spin decoherence?).

The discussion so far has not allowed for the dependence of proton revolution time on betatron oscillation amplitude. Before considering spin precession one can rethink the effect of a systematic energy deviation from design of an injected beam. We know from experience with storage rings that the beam will automatically adjust its average radius so that its average revolution period matches the RF frequency. If the discrepancy is too great some or all of the beam will strike the chamber wall and be lost. With counter-circulating beams the situation is the same but, because the beams have not quite the same average energy, their overlap will be imperfect. Here, where we are concentrating on the effect of betatron oscillations, we ignore this complication.

Consider first the effect of purely vertical betatron oscillations on the longitudinal equilibrium. There can be no doubt that the circumference of an orbit that oscillates above and below the horizontal median plane, while staying at the same radius, is longer than the circumference of its projection onto the median plane. And yet the RF forces these orbits, on the average, to have the same period. Unless something is done about it, this would force the velocities of these orbits to depend on their vertical betatron amplitudes. This would, in turn, lead to the inexorable growth of the (relative) polarization angle α . Before thinking about what can be done about it, we can estimate the drift rate. For a particle with slope $y' (\equiv dy/ds)$, the total velocity β and in-plane velocity β_{horz} are related (in paraxial approximation) by

$$\beta^2 = \beta_{\text{horz}}^2 (1 + y'^2). \quad (148)$$

Protons of average r.m.s. slope $\langle y'^2 \rangle$ therefore, on the average, have velocities

$$\beta(\langle y'^2 \rangle) = \beta_0 + \frac{1}{2} \beta_0 \langle y'^2 \rangle, \quad (149)$$

where β_0 is the average in-plane velocity enforced by the RF. According to Eq. (133), this altered velocity will alter the precession rate by the amount

$$\Delta \frac{d\alpha}{dt} = \frac{eE}{m_p c} \left(\frac{g\beta_0}{2} + \frac{1}{\beta_0} \right) \frac{\Delta\beta}{\beta_0} = \frac{\gamma_0 E c}{p_0 c/e} \langle y'^2 \rangle. \quad (150)$$

(A simplifying trick is handy here: since the two terms in parenthesis cancel when there is a minus sign (that is the magic condition) they must be equal with a positive sign after differentiation.) In a weak focusing ring the accelerator lattice beta function $\beta_y^{\text{latt.}}$ is constant with approximate value

$$\beta_y^{\text{latt.}} \approx \frac{C_0}{2\pi Q_y}, \quad (151)$$

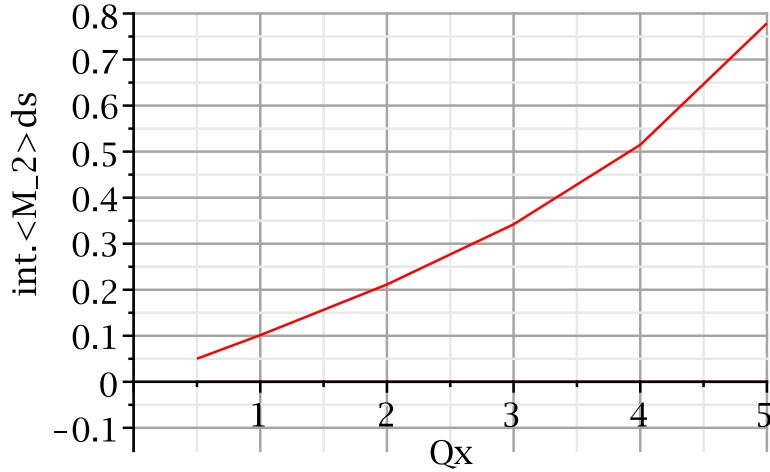


Figure 8: Excess path length coefficient $\int \langle M_2 \rangle_{\psi_{x,0}} ds$ plotted as a function of tune Q_x , holding the circumference constant, for an equal tune FODO lattice.

and the r.m.s. displacements and slopes are related to the vertical emittance by

$$\langle y'^2 \rangle = \frac{\langle y^2 \rangle}{\beta_{\text{latt.}}^2} = \frac{\epsilon_y}{\beta_y^{\text{latt.}}} = \frac{2\pi Q_y}{C_0} \epsilon_y. \quad (152)$$

Substitution into Eq. (150) yields

$$\frac{d}{dt} \alpha^{(\text{one sigma})} = \frac{\gamma_0 E c}{p_0 c / e} \frac{2\pi Q_y}{C_0} \epsilon_y \quad (153)$$

$$\left(\text{e.g. } \frac{1.25 \times (17 \times 10^6) \times (3 \times 10^8)}{0.7 \times 10^9} \frac{2\pi \times 0.5}{300} 1.0 \times 10^{-6} \right) = 0.1 \text{ r/s.}$$

This decoherence rate (if it were the only contributor) would limit run lengths to about 10 seconds, which is some two orders of magnitude shorter than the nominally specified run time. Incidentally, the factor Q_y in the final numerator factor suggests that low tune lattices may be favored.

This issue is analysed quantitatively in Appendix A.1 in which an analytic excess path length formula is derived. When applied to the equal tune FODO lattice one obtains the tune dependence shown in Fig. 8. This plot confirms that low tune values in both planes are desirable for minimizing betatron-induced decoherence.

Recapitulating, since the RF enforces equal revolution time, variation of path length implies deviant velocity, which causes spin decoherence. It is possible to cancel the dependence implied by $\langle M_2 \rangle$ using sextupoles. Apart from the fact that sextupoles can cause other complications (which favors weak sextupoles)

for a given fractional compensation precision, the eventual decoherence time varies inversely with $\langle M_2 \rangle$. From this point of view it can be seen that low betatron tunes are favored for the EDM experiment.

10 Curved-Planar (Weak) Separated Function FODO Lattice

The eventual practical proton EDM ring will require long straight sections for injection, RF cavity, dispersion suppression, and so on, for example as shown in Fig. 11. But for initial decoherence studies the simplest ring to study is purely circular. Such a ring is identical to the ring shown in Fig. 11, but with the long straight sections removed. Another simplification is to treat the quadrupoles and sextupoles as thin elements. As discussed elsewhere in the report, another requirement is for both betatron tunes to be as small as is practical. These last two points mesh nicely, since the required quadrupole focal lengths will be long, permitting the quad lengths to be short.

For spin decoherence compensation one requires at least three families of sextupoles. A continuous bend is therefore unsatisfactory. This has led to the design shown in Table 2 and in Figures 9 through 18, and the following table of lattice functions. The FODO quad locations are labelled A and B.

NAME	S	BETX	ALFX	BETY	ALFY	DX	PSIX/(2 pi)	PSIY/(2 pi)
	m	m		m		m		
"A"	0.000	29.678	0.0000	21.440	0.0000	21.547	0.0000000	0.00000
"QUADA"	0.001	29.677	0.9378	21.440	-0.6776	21.547	0.0000053	0.0000074
"SEXTA"	0.0015	29.676	0.9378	21.441	-0.6776	21.547	0.0000080	0.0000111
"BEND"	0.0015	29.676	0.9378	21.441	-0.6776	21.547	0.0000080	0.0000111
"BENDH"	2.500	25.221	0.8416	25.252	-0.8477	19.879	0.0145481	0.0171336
"C"	2.500	25.221	0.8416	25.252	-0.8477	19.879	0.0145481	0.0171336
"SEXTC"	2.5005	25.220	0.8416	25.253	-0.8477	19.878	0.0145513	0.0171367
"BENDH"	4.9990	21.299	0.7247	29.914	-1.0177	18.284	0.0317240	0.0316247
"BEND"	4.9990	21.299	0.7247	29.914	-1.0177	18.284	0.0317240	0.0316247
"SEXTB"	4.9995	21.298	0.7247	29.915	-1.0178	18.284	0.0317278	0.0316274
"B"	5.0005	21.298	0.0000	29.916	0.0000	18.284	0.0317353	0.0316327

Compensation of spin decoherence is discussed in Section 12. One quantity that will be needed there (for both planes) is $\int_0^{\ell_C} \gamma ds$, where $\ell_C = 2\ell = 10$ m is the length of a full cell. Treating the bend regions as drifts (for purposes of focusing calculations) $\gamma_x = (1 + \alpha^2)/\beta_x$ and γ_y are constant through the bend region. They can be therefore be evaluated at point C. As a result

$$\begin{aligned}
 \int_0^{\ell_C} \gamma_x ds &\approx \ell_C \gamma_x(C) = 10.0(1 + 0.8416^2)/25.221 = 0.6773, \\
 \int_0^{\ell_C} \gamma_y ds &\approx \ell_C \gamma_y(C) = 10.0(1 + 0.8447^2)/25.252 = 0.6786.
 \end{aligned}
 \tag{154}$$

Table 2: EDM electrostatic lattice parameters. Some entries are evaluated in a later section. This lattice will prove to be unsatisfactory because the magic γ and the transition γ very nearly coincide.

quantity	symbol	unit	value
number of full cells	N_C		20
half-cell length	ℓ	m	5.0
circumference	$\ell_0 = 2N_C\ell$	m	200
horz. foc. half quad str.	q_A	1/m	0.0316013
horx. defoc. half quad str.	q_B	1/m	-0.0340228
horizontal tune	Q_x		1.2694
vertical tune	Q_y		1.2653
achromatic sext. strengths	$S_{\text{achrom.}}^A$	1/m ²	0.001411
	$S_{\text{achrom.}}^B$	1/m ²	-0.001790
spin compensated sextupole strengths	$S_{\text{sp.com.}}^A$	1/m ²	0.0017131
	$S_{\text{sp.com.}}^B$	1/m ²	-0.0023739
	$S_{\text{sp.com.}}^C$	1/m ²	-0.00033436

(It is somewhat coincidental that these values are so close. The tunes and beta functions in any eventually-adopted lattice are likely to be far less equal.

The three sextupole family requirement is met by the presence of sextupole slots at the A and B locations, as well as at C points at the centers of every bend element. For really small tunes the beta and dispersion functions would be more or less constant around the ring which would not provide the necessary distinction among the A, B, and C locations. To magnify the scalloping of the lattice functions, a lengthened cell length is suggested. As can be seen from Fig. 11, there are 10 cells per arc, which is only half as many as has been assumed in earlier (magnetic) EDM lattices. Preliminary studies show that there is then sufficient distinction among the A, B, and C points to avoid the need for special purpose, high beta, compensation sections. This represents a significant reduction in complexity.

The final two columns of the table give the tune advances per cell in horizontal and vertical planes. With 20 full cells in all, the resulting tunes are $Q_x = 20 \times 0.03173 = 1.2694$ and $Q_y = 1.2653$, essentially equal. This is not necessarily appropriate, but it seems like a satisfactory starting situation.

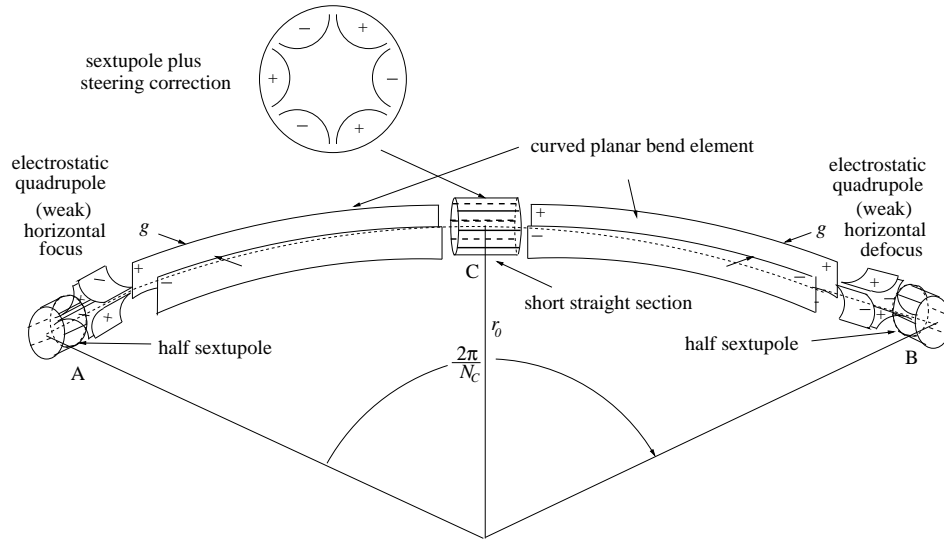


Figure 9: One half cell of a weak FODO lattice with curved-planar electrodes. In the thin lens model the quadrupole and sextupole elements are treated as thin elements at lattice points A, C, and B.

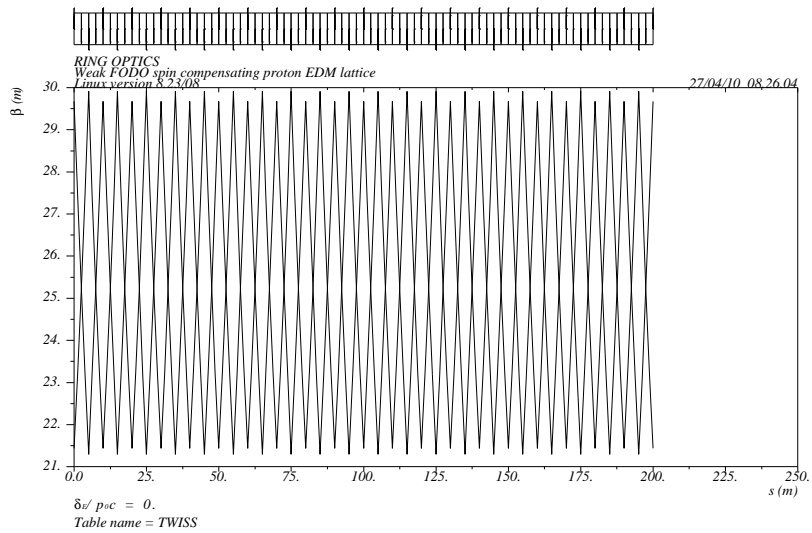


Figure 10: Weak FODO, full ring beta functions

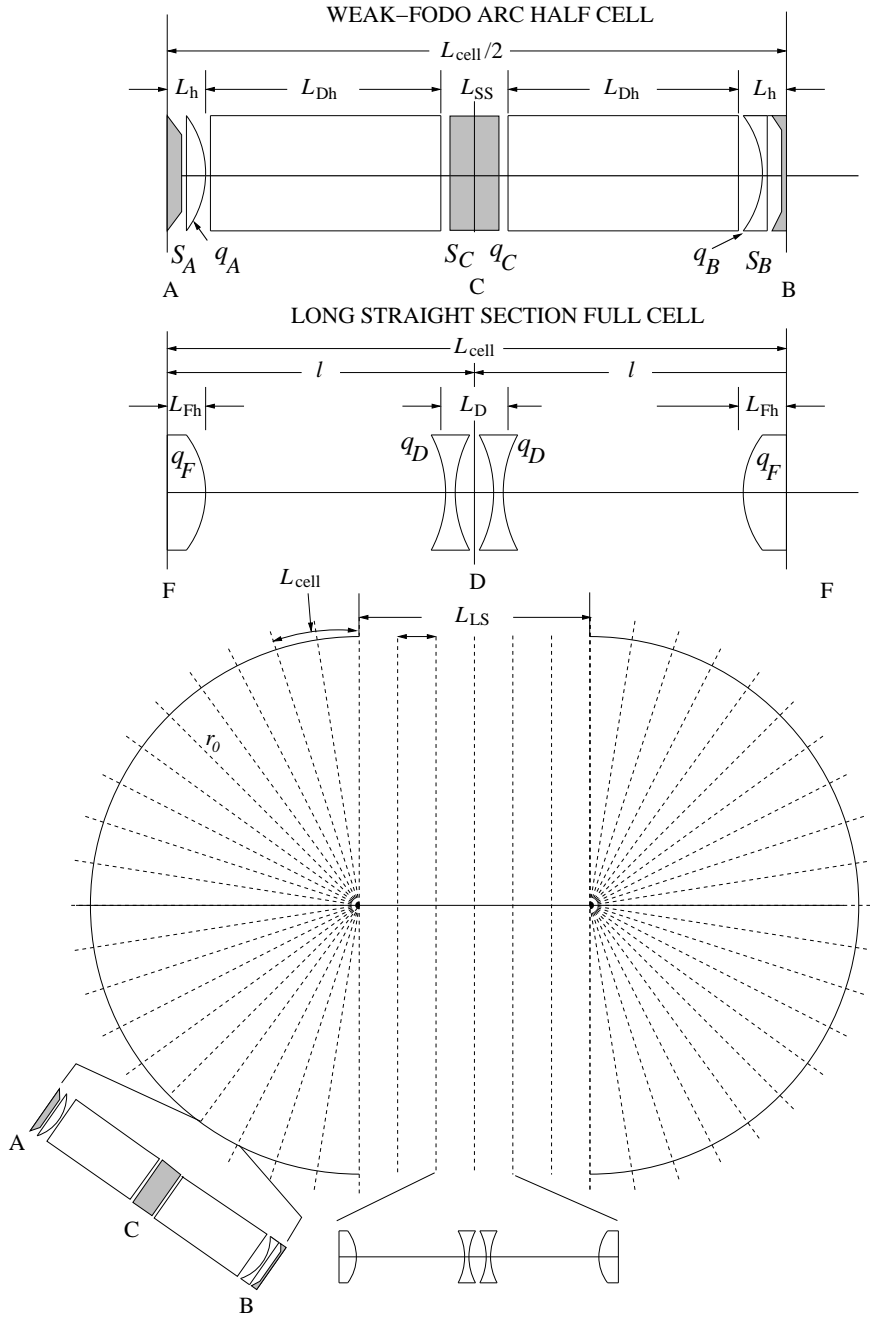


Figure 11: Labels and lengths of an arc half cell and a long straight section full cell of weak FODO lattice. q_C is not a true quadrupole; it represents the excess (electrostatic) focusing effect of the bend element. Sextupole elements are shown shaded. The full ring is sketched, with long straight sections having (tentatively) an odd number (3) of full FODO cells. There are 10 full cells in each arc.

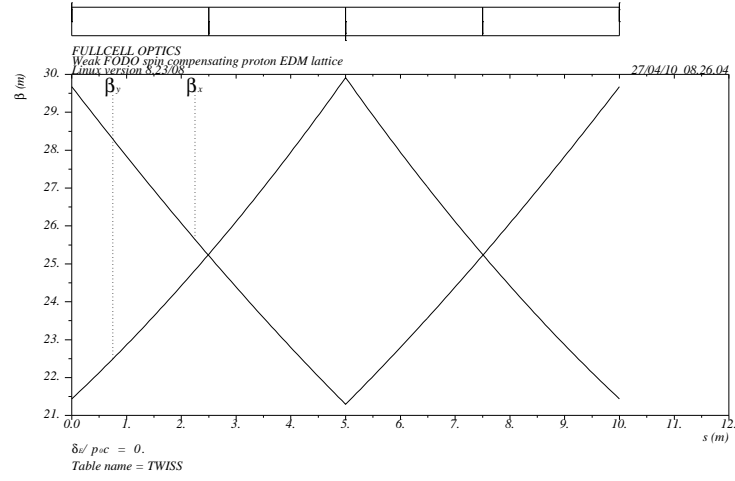


Figure 12: Weak FODO, single cell beta functions

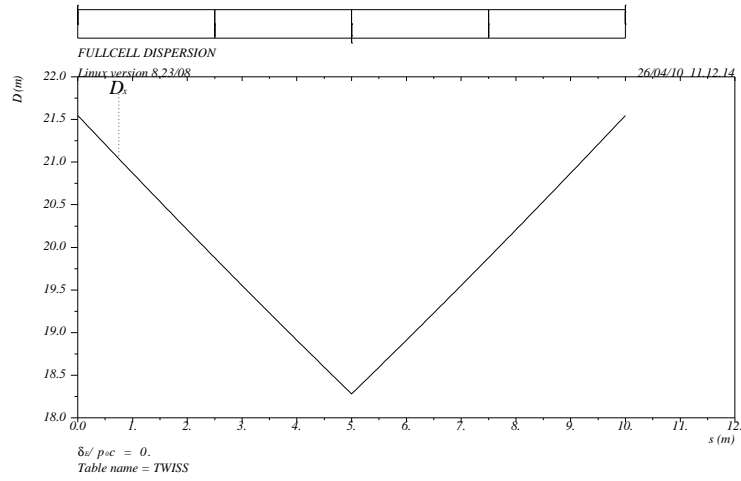


Figure 13: Weak FODO, single cell beta dispersion

11 Qualitative Discussion of Betatron-Induced Decoherence

For the EDM experiment to succeed it will be necessary to compensate the lattice to reduce the decoherence rate calculated in Eq. (153) (and other) sources of decoherence. We can regard Eq. (153) as providing the next to lowest order term of a series in powers of the dimensionless ratio $y/\beta_y^{\text{latt.}} \sim \sqrt{\epsilon_y/\beta_y^{\text{latt.}}} \sim 10^{-3}$. A compensation scheme cancelling the effect to this order could, in principle, reduce the precession rate by a factor of about one thousand. As a matter of fact, since, by up-down symmetry, expansions in y invariably have only odd powers of y , the compensation of vertically-induced decoherence could be even better. But horizontally-induced decoherence (over and above what is momentum-correlated) will be at least as important as vertically-induced, and no such restriction to even powers is guaranteed.

To prevent the inexorable drift of α calculated previously, we have to prevent $\beta_{\text{horz.}}$ from changing as a function of vertical betatron amplitude $\sqrt{\langle y^2 \rangle}$. It does not do any good to have tailored the local \mathbf{E} -field shape judiciously, since momentum and polarization precession rates have the same dependence on \mathbf{E} . The only way to change $\beta_{\text{horz.}}$ is to shorten the path length proportionally with $\langle y^2 \rangle$. Only in this way can the magic speed can be retained.

In an EDM note dated 10 October, 2004, (for deuteron EDM) Yuri Orlov explains how sextupoles in the ring can provide this kind of compensation. Yuri's treatment of momentum-dependent compensation is not quite the same as mine (explained in Section 8.1). This complicates comparison of his treatment with mine. But, to the extent they are both correct, at some basic level the two treatments have to be roughly equivalent. Yuri points out that it is impossible to match three conditions (from three phase space axes, longitudinal, horizontal, and vertical) with a simple FODO lattice, which has places for only two families of sextupoles.

A possible workaround for this would be to fully couple horizontal and vertical betatron motions. The simplest way to do this is to run "on the coupling resonance". (I recall from some pEDM presentation, that accurate decoupling is important for the EDM measurement. But I do not remember why.) As long as the sloshing rate between modes is rapid compared to the decoherence rate any precession drift while the vertical betatron amplitude is large can be cancelled by opposite drift when the horizontal amplitude is large. This option is possibly worth exploring but, for now, I assume that at least three families of sextupoles will be required.

An optimist might note that there will inevitably be sloshing between horizontal and longitudinal modes. If this represented ideal "mixing" in phase space, one could hope that the spin decoherence would be somewhat reduced. But any such mixing is incomplete. For example, in the mixing between horizontal and vertical, the sum of Courant-Snyder invariants $W_x + W_y$ is preserved. And there are no doubt similar preserved invariants in six dimensions.

One could induce intentional mixing by interchanging small and large am-

plitudes in phase space, perhaps by discontinuous frequency modulation of the RF frequency. But this would probably lead to unacceptable emittance growth. One (unavoidable) source of mixing, is intrabeam scattering (IBS). To the extent this causes inexorable and unwelcome emittance growth, it could also lead to some welcome decrease in spin decoherence (assuming that individual IBS scatters are spin independent.)

Lattices discussed in the previous, version I, of this report, had the possibility of at least three independent sextupole families, with two of the families assumed to be in special compensating sectors of the lattice. Since those lattices had high tunes they have been jettisoned from this version. Furthermore, to avoid the complication of special compensation sectors, it now seems preferable to have the compensation distributed uniformly through the arc cells. Low tunes have also resulted in another simplification. Because only weak focusing is required, it is unnecessary to use toroidal-shaped bending electrodes.

12 Betatron Decoherence Compensation

The main formulas needed for compensating the lattice against spin decoherence are given in the appendices. The betatron-induced excess path lengths $\Delta\ell_x(\epsilon_x)$ and $\Delta\ell_y(\epsilon_y)$ are given by Eqs. (189) and (190); they are to be compensated by sextupoles.

With the horizontal angular deflection caused by a sextupole of strength S being given by

$$\theta_x = -\frac{1}{2} S (x^2 - y^2), \quad (155)$$

the average angular deflection is

$$\langle\theta_x\rangle = -\frac{1}{2} S \langle(x^2 - y^2)\rangle = -\frac{1}{2} S (\epsilon_x\beta_x - \epsilon_y\beta_y). \quad (156)$$

(The sign of S here has been chosen so that, with increasing x , a sextupole with positive S *strengthens* the focusing of a superimposed quadrupole with positive q .) One must be certain that the emittances ϵ_x and ϵ_y introduced here are identical to the emittances ϵ_x and ϵ_y appearing in Eqs. (189) and (190). The excess path length $\Delta\ell(\theta_{x,j})$ caused by horizontal deflections $\theta_{x,j}$ at locations j is given by Eq. (196);

$$\Delta\ell(\theta_{x,j}) = D(s_j) \theta_{x,j}, \quad (157)$$

which averages to

$$\langle\Delta\ell(\theta_{x,j})\rangle = -\frac{D(s_j) S_j}{2} (\epsilon_x\beta_{x,j} - \epsilon_y\beta_{y,j}) \quad (158)$$

The condition for path lengths to cancel on the average is

$$\Delta\ell_x(\epsilon_x) + \Delta\ell_y(\epsilon_y) = -\sum_j \Delta\ell(\theta_{x,j}), \quad (159)$$

or

$$\frac{\epsilon_x}{4} \int_0^{\ell_0} \gamma_x ds + \frac{\epsilon_y}{4} \int_0^{\ell_0} \gamma_y ds = \sum_j \frac{D(s_j) S_j}{2} (\epsilon_x \beta_{x,j} - \epsilon_y \beta_{y,j}). \quad (160)$$

To satisfy this condition for all possible combinations of ϵ_x and ϵ_y , this single condition reduces to two conditions;

$$\begin{aligned} \int_0^{\ell_0} \gamma_x ds &= 2 \sum_j D(s_j) S_j \beta_{x,j}, \\ \int_0^{\ell_0} \gamma_y ds &= -2 \sum_j D(s_j) S_j \beta_{y,j}. \end{aligned} \quad (161)$$

Though possible, it is rare for the dispersion to be negative. We assume $D(s_j) > 0$ and even, for qualitative argument, that $D(s_j)$ is roughly constant, independent of j . Then, of the factors occurring in these conditions, the only one that can be negative is S_j . To meet the second condition, clearly some of the S_j values have to be negative. To meet the conditions simultaneously we will need the S_j values to be large and positive at points where $\beta_{x,j}$ is large (compared to $\beta_{y,j}$), and we will need the S_j values to be large and negative at points where $\beta_{y,j}$ is large (compared to $\beta_{x,j}$).

For now we assume the ring consists of N_C identical cells, with identical compensation in each cell. The compensating deflections are to be caused by sextupole families A, B, and C, with N_C identically-powered and situated sextupoles in each family. Then Eqs. (161) reduce to

$$\begin{aligned} \frac{1}{2N_C} \int_0^{\ell_0} \gamma_x ds &= D^A S^A \beta_x^A + D^B S^B \beta_x^B + D^C S^C \beta_x^C, \\ -\frac{1}{2N_C} \int_0^{\ell_0} \gamma_y ds &= D^A S^A \beta_y^A + D^B S^B \beta_y^B + D^C S^C \beta_y^C. \end{aligned} \quad (162)$$

At this point we can also restore ‘‘sextupole chromatic neutrality’’, as discussed in Appendix A.3, by imposing the condition

$$S^A D^{A^3} + S^B D^{B^3} + S^C D^{C^3} = 0. \quad (163)$$

For a given lattice configuration, the task is to solve these equations for S^A , S^B , and S^C .

$$\begin{pmatrix} D^A \beta_x^A & D^B \beta_x^B & -D^C \beta_x^C \\ D^A \beta_y^A & D^B \beta_y^B & -D^C \beta_y^C \\ D^{A^3} & D^{B^3} & D^{C^3} \end{pmatrix} \begin{pmatrix} S^A \\ S^B \\ S^C \end{pmatrix} = \begin{pmatrix} \frac{1}{2} \int_0^{\ell_C} \gamma_x ds \\ -\frac{1}{2} \int_0^{\ell_C} \gamma_y ds \\ 0 \end{pmatrix}. \quad (164)$$

In the final form the ranges of integration have been reduced from the full ring circumference to the single cell length $\ell_C = \ell_0/N_C$. In this form individual cells

can be thought of as self-compensating. When the lattice is made more realistic, for example by the addition of long straight sections, these values can be used for first approximation. Eventually, though, the equations will have to be solved for the whole lattice.

Copying numerical values from Section 10, Eq. (164) becomes

$$\begin{pmatrix} 21.547 \times 29.678 & 18.284 \times 21.298 & -19.879 \times 25.221 \\ 21.547 \times 21.440 & 18.284 \times 29.916 & -19.879 \times 25.262 \\ 21.547^3 & 18.284^3 & 19.879^3 \end{pmatrix} \begin{pmatrix} S^A \\ S^B \\ S^C \end{pmatrix} = \begin{pmatrix} 0.6773/2 \\ -0.6786/2 \\ 0 \end{pmatrix}. \quad (165)$$

Solving this equation yields

$$S^A = 0.0017131 \quad (166)$$

$$S^B = -0.0023739 \quad (167)$$

$$S^C = -0.00033436 \quad (168)$$

Another approach that can be taken is to leave S^C as a free parameter, and solve the first two equations for S^A and S^B . This approach yields

$$\begin{aligned} S^A &= 0.4636S^C + 0.0018681, \\ S^B &= 0.5262S^C - 0.0021980. \end{aligned} \quad (169)$$

From the small value of S^C , or by comparing Eqs. (168) and (169), one sees that the chromatic effects of A and B are quite small.

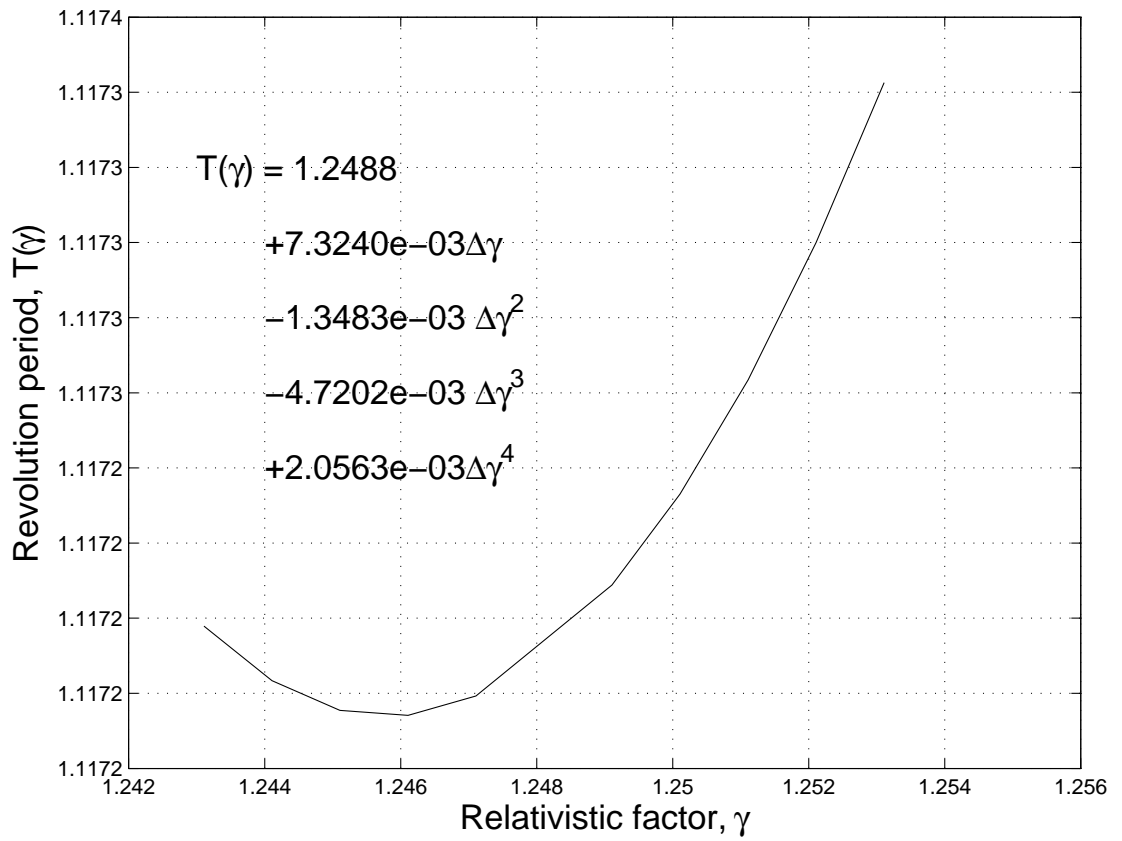


Figure 14: Plot of uncompensated revolution period $T(\gamma)$ as a function of γ for the weak focusing FODO lattice with $S^C = 0$, $Q_x = 1.2694$, $Q_y = 1.2653$.

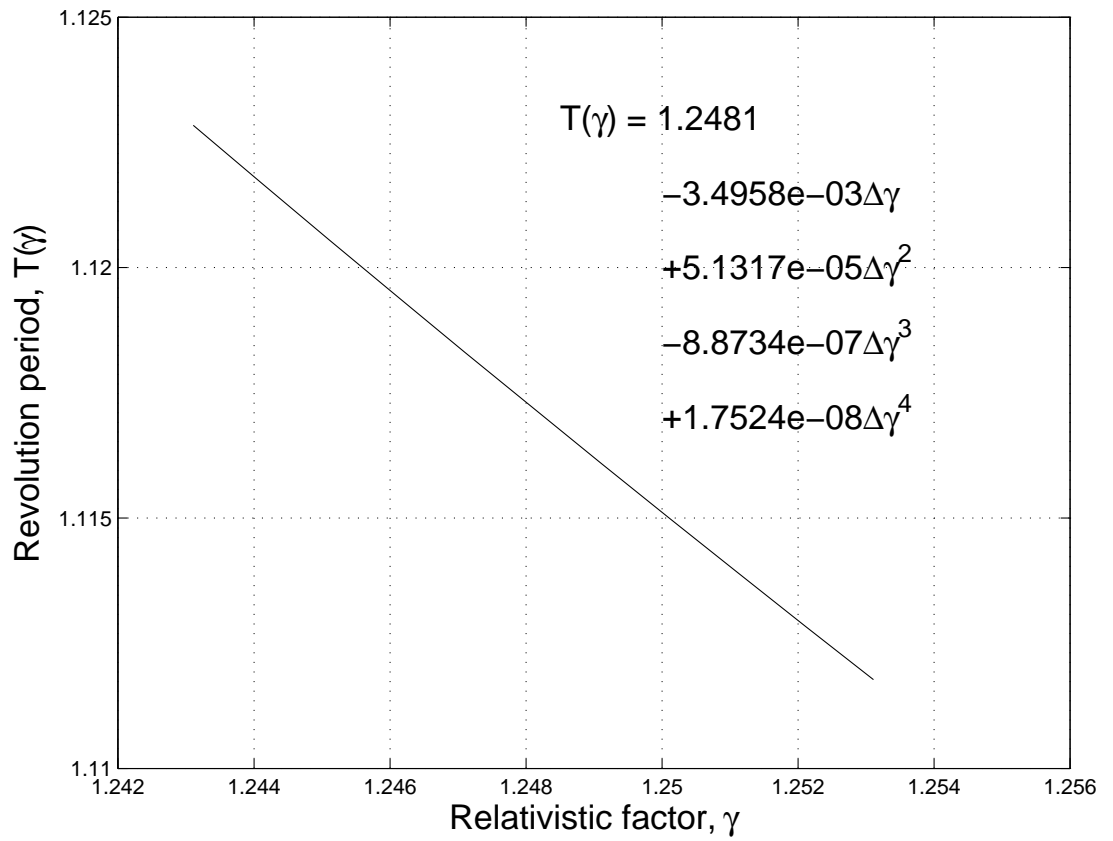


Figure 15: Plot of uncompensated revolution period $T(\gamma)$ as a function of γ for the weak focusing FODO lattice with $S^C = 0$, $Q_x = 2.2585$, $Q_y = 1.2566$.

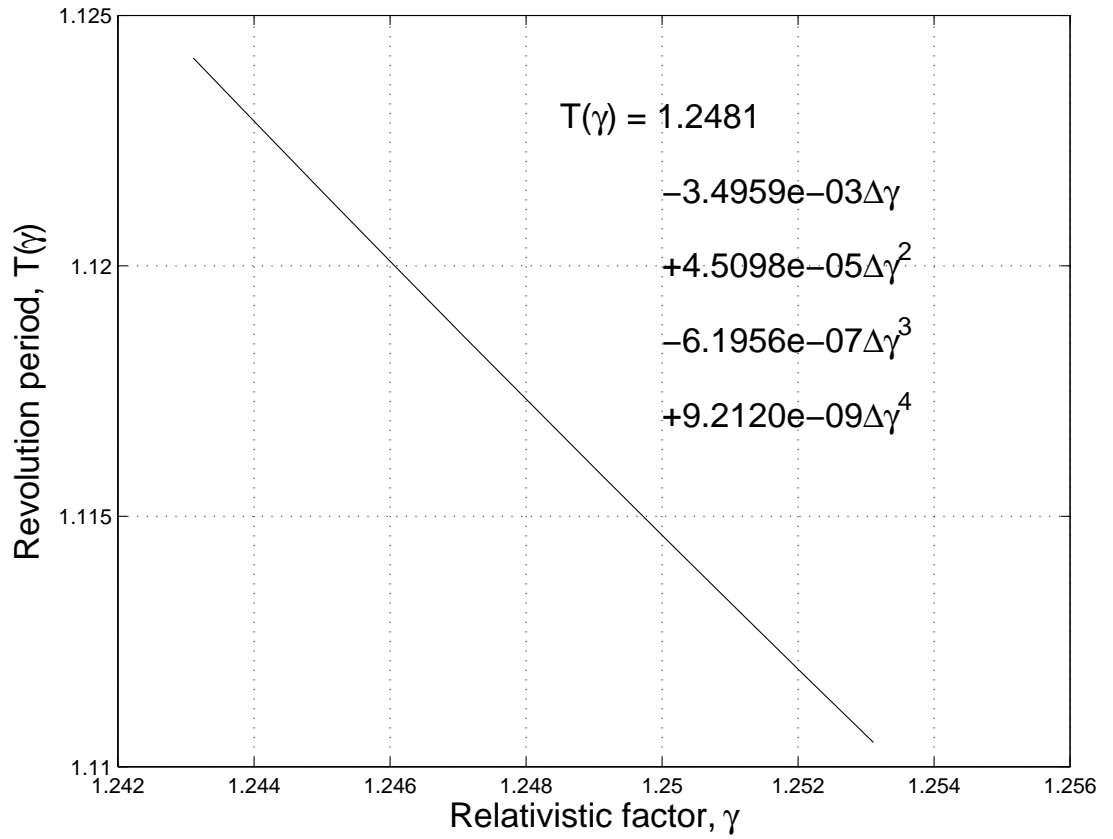


Figure 16: Plot of uncompensated revolution period $T(\gamma)$ as a function of γ for the “less weak” focusing FODO lattice, $Q_x = 3.2547$, $Q_y = 1.2566$, with sextupoles turned off.

13 Curved-Planar (Less Weak) Separated Function FODO Lattice and Incorporation of Long Straight Sections

From the discussion of Section 12 and figures 14 through 16 it seems clear that the horizontal tune has to be increased substantially from its earlier assumed low value. Of the three cases studied previously we pick the highest horizontal tune case and refer to it as the “less weak” case. Its $T(\gamma)$ dependence is shown in Fig. 16, along with its expansion in powers of $\Delta\gamma = \gamma - \gamma_0$. As explained earlier the constant and linear terms are harmless. The first term leading to decoherence is $4.5 \times 10^{-5} \Delta\gamma^2$.

The experiment will also need long straight sections, for injection, RF, polarimetry, and so on. Commonly one incorporates dispersion suppression causing the dispersion to vanish through the long straights. Even with serious effort I have been unable to design such dispersion suppression, without using strong bends which mangling the decoherence compensation. I conclude it is necessary to “manage” the dispersion. That is to say to “match it through the long straights, to the previously designed arcs. The decoherence compensation will still have to be re-done (after more realistic straights are specified) but the changes should be quite minor.

Parameters of the full ring are given in the following tables and figures.⁷ The lattice layout was shown earlier in Fig. 11. The tunes are $Q_x = 5.20$ and $Q_y = 1.75$. Including phase advances in the long straights, these are larger than the tunes listed in the caption of Fig. 16.

NAME	S	BETX	ALFX	BETY	ALFY	DX	PSIX/(2 pi)	PSIY/(2 pi)
	m	m		m		m		
"A"	0.0000	15.1937	0.0000	17.8478	-0.0000	3.7688	0.0000000	0.0000000
"QUADA"	0.0010	15.1925	1.2309	17.8492	-1.4462	3.7687	0.0000105	0.0000089
"SEXTA"	0.0015	15.1912	1.2308	17.8507	-1.4463	3.7685	0.0000157	0.0000134
"BEND"	0.0015	15.1912	1.2308	17.8507	-1.4463	3.7685	0.0000157	0.0000134
"BENDH"	2.5000	10.0038	0.8411	26.1591	-1.8791	3.0928	0.0324636	0.0184564
"C"	2.5000	10.0038	0.8411	26.1591	-1.8791	3.0928	0.0324636	0.0184564
"SEXTC"	2.5005	10.0030	0.8410	26.1610	-1.8792	3.0927	0.0324715	0.0184595
"BENDH"	4.9990	6.8194	0.4306	36.6324	-2.3119	2.5941	0.0813320	0.0313186
"BEND"	4.9990	6.8194	0.4306	36.6324	-2.3119	2.5941	0.0813320	0.0313186
"SEXTB"	4.9995	6.8190	0.4305	36.6347	-2.3120	2.5940	0.0813437	0.0313208
"QUADB"	5.0005	6.8186	0.0000	36.6370	-0.0000	2.5939	0.0813670	0.0313252
"B"	5.0005	6.8186	0.0000	36.6370	-0.0000	2.5939	0.0813670	0.0313252

⁷Question from recent weekly conference call: “What is the slip factor η_0 ?”. It is related to the so-called transition gamma γ_t by

$$\eta_0 = \frac{1}{\gamma_t^2} - \frac{1}{\gamma_0^2} = \frac{1}{3.668^2} - \frac{1}{1.25^2} = -0.566. \tag{170}$$

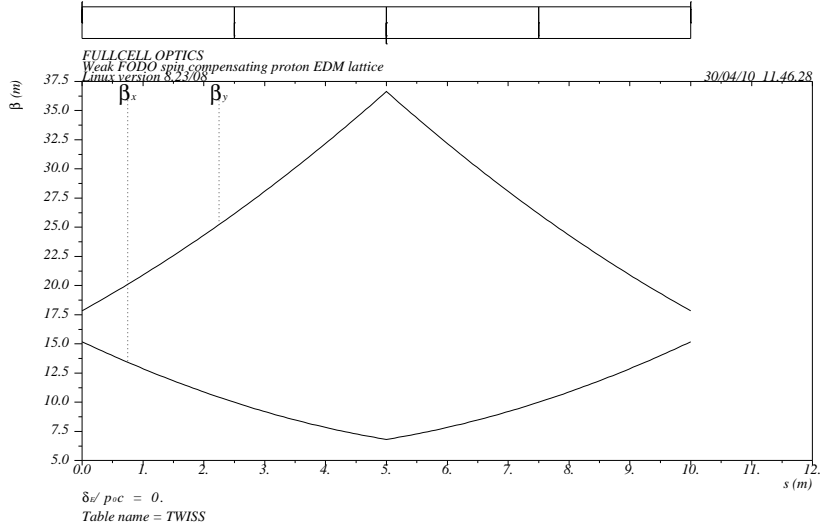


Figure 17: Less weak FODO, single cell beta functions

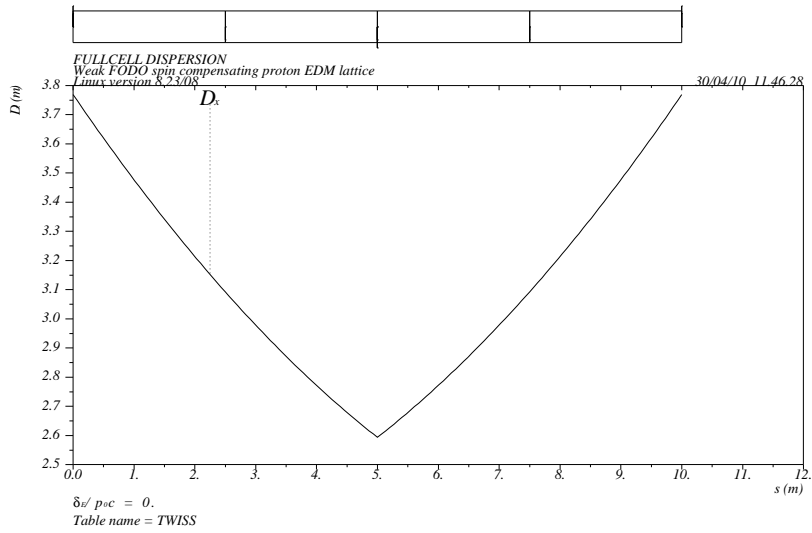


Figure 18: Less weak FODO, single cell beta dispersion

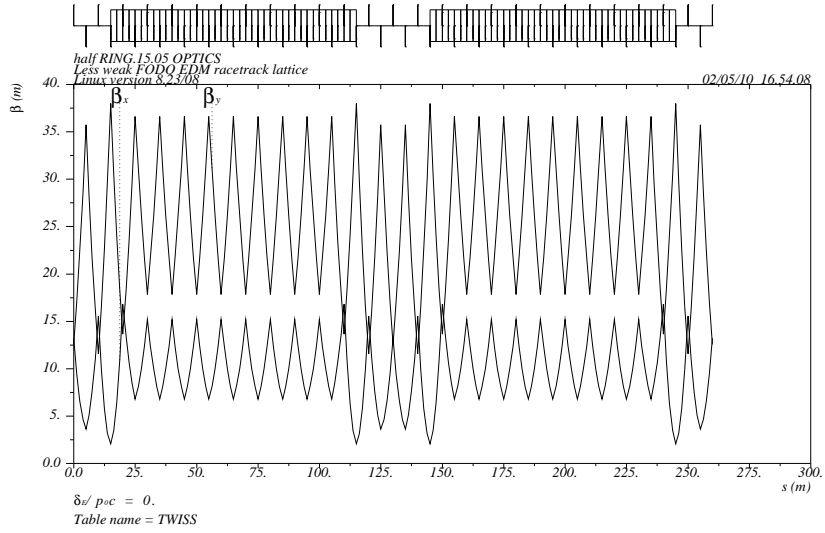


Figure 19: Beta functions for full racetrack ring with dispersion “managed” in the long straight sections.

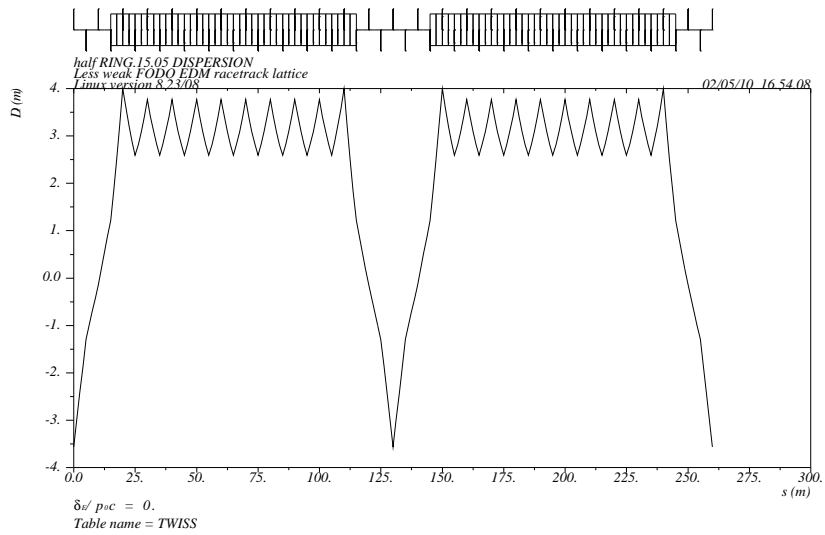


Figure 20: Dispersion function for full racetrack ring with dispersion “managed” in the long straight sections.

Table 3: EDM electrostatic lattice parameters for the “less weak” option, including long straight sections.

quantity	symbol	unit	value
number of arc cells	N_C		20
number of arc cells	N_{ss}		6
half-cell length	ℓ	m	5.0
circumference	$\ell_0 = 2(N_C + N_{ss})\ell$	m	260.006
horz. foc. half quad str.	q_A	1/m	0.08102
horx. defoc. half quad str.	q_B	1/m	-0.06311
horizontal tune	Q_x		5.1999
vertical tune	Q_y		1.7495
transition γ	γ_t		3.668
achromatic sext. strengths	$S_{\text{achrom.}}^A$	1/m ²	0.02127
	$S_{\text{achrom.}}^B$	1/m ²	-0.02406
spin compensated sextupole strengths	$S_{\text{sp.com.}}^A$	1/m ²	0.01802
	$S_{\text{sp.com.}}^B$	1/m ²	-0.03303
	$S_{\text{sp.com.}}^C$	1/m ²	-0.01312

14 Numerical Examples

Corresponding to $\pm\Delta\gamma$ the range of fractional momenta is

$$\pm \frac{\Delta p}{p} = \pm \frac{\mathcal{E}^2}{p^2} \frac{\Delta\gamma}{\gamma} = \pm \frac{\Delta\gamma}{\beta^2\gamma} = \pm 2.238\Delta\gamma. \quad (171)$$

According to Eq. (141), the polarization angle α of an individual proton sweeps fast (at the synchrotron oscillation frequency) back and forth through a range

$$\pm\alpha_{\max}^{(F)} = \pm 3.586 \frac{\Delta\gamma_{\max}}{Q_s} = \pm 1.60 \frac{(\Delta p/p)_{\max}}{Q_s}. \quad (172)$$

This motion causes no decoherence but, if the range is too great, the secular vertical precession due to the electric dipole moment, whose measurement is the purpose for the experiment, will be unacceptably reduced. Let $\alpha_{\max-\max} \stackrel{\text{say}}{=} 0.5$ r be an arbitrarily-assigned, maximum acceptable excursion angle.

At this point it seems prudent to compare with previous formulations of the synchrotron oscillation modulated spin precession. Eq. (3) on page 7 of the pEDM experimental proposal[7], gives

$$\omega_{\mathbf{a}} = -\frac{e}{m_p} \left(\frac{g}{2} - \left(1 + \left(\frac{m_p c^2}{pc} \right)^2 \right) \right) \frac{\beta \times \mathbf{E}}{c} \quad (173)$$

as the anomalous precession rate. With β perpendicular to \mathbf{E} , taking absolute values, and identifying $\omega_a = d\alpha/dt$, this reduces to our Eq. (133). According to Eq. (10) in the same pEDM proposal, the deviant precession rate caused by a deviant fractional momentum ($\Delta p/p$) is given by

$$\begin{aligned} \frac{d}{dt} \Delta\alpha &= \frac{Ec}{m_p c^2/e} \left(2\beta \left(\frac{m_p c^2}{pc} \right)^2 \right) (\Delta p/p) = \frac{Ec}{m_p c^2/e} \left(\frac{2}{\beta\gamma^2} \right) (\Delta p/p) \\ &= \frac{(17 \times 10^6) \times (3 \times 10^8)}{0.938 \times 10^9} \left(\frac{2}{0.6 \times (1.25)^2} \right) (\Delta p/p) \\ &= 1.16 \times 10^7 (\Delta p/p). \end{aligned} \quad (174)$$

For example, during a revolution time of 10^{-6} s, a fractional momentum offset of 0.001 would cause a precession angle deviation of 0.0116 r. (In an estimate dated April 2, 2010, Bill Morse, for time = 10^{-6} s, $\Delta\beta = 0.001$, gets a precession angle deviation of 0.028 r. I get that $\Delta\beta = 0.001$ corresponds to fractional momentum offset of 0.0026. For this case Eq. (174) gives 0.030 r, in quite good agreement with Bill's value.)

During synchrotron oscillation at synchrotron tune Q_s the fractional momentum offset is given by

$$(\Delta p/p) = (\Delta p/p)_{\max} \sin(2\pi Q_s t/T_0). \quad (175)$$

Substituting this into Eq. (174) and integrating gives

$$\begin{aligned}\Delta\alpha &= 1.16 \times 10^7 (\Delta p/p)_{\max} \int_0^t dt' \sin(2\pi Q_s t'/T_0) \\ &= -\frac{1.16 \times 10^7 T_0}{2\pi Q_s} (\Delta p/p)_{\max} \cos(2\pi Q_s t/T_0)\end{aligned}\quad (176)$$

Taking $T_0 = 1 \mu\text{s}$ as a typical revolution period, this determines the ratio

$$\frac{Q_s}{(\Delta p/p)_{\max.}} = \frac{1.16 \times 10^7 T_0}{2\pi\alpha_{\max-\max.}} = \frac{11.6}{\pi} = 3.69.\quad (177)$$

The same line of reasoning applied to Eq. (172) yields

$$\frac{Q_s}{(\Delta p/p)_{\max}} = \frac{1.60}{\alpha_{\max-\max.}^{(F)}} = \frac{1.60}{0.5} = 3.20.\quad (178)$$

This agrees fairly well with the preceding determination. Setting aside the question “why do they not agree exactly” ($\mu_s \ll 1$ approximation?) one can note from the latter determination that the ratio is independent of electric field, RF frequency, and revolution period.

Based on limiting the momentum-correlated precession range, there is no reason for Q_s to be larger than needed to satisfy Eq. (178). Increasing Q_s from there, for example to obtain shorter bunch length, would reduce the precession range beneficially.

Correlating with candidate injected beam momentum spread values from a Semertzidis note dated 14 March, 2010, one obtains the values shown in Table 4. The upper two rows correspond more closely to entries in a table due to Alexei Fedotov, to be discussed below. From Eqs. (171) and (178) and formulas in Section 8.1 one has

$$\begin{aligned}\Delta\gamma_{\max.} &= 0.4468 (\Delta p/p)_{\max}, \\ Q_s &= 1.60 \frac{(\Delta p/p)_{\max}}{\alpha_{\max-\max}}, \\ \hat{V}_{RF} &= G_{RF} \mu_s (m_p c^2/e) \Delta\gamma_{\max}, \\ t_{\max} &= \frac{1}{\omega_{RF}} \frac{1}{G_{RF}}, \\ \ell_{\max} &= 0.598 ct_{\max}.\end{aligned}\quad (179)$$

These formulas do not fix G_{RF} , which is a number that has to be substantially larger than 1 for the linearized treatment of synchrotron motion to be accurate. The numerical values in Table 4 assume $G_{RF} = 2$, $\alpha_{\max-\max} = 0.5$, and $\omega_{RF}/(2\pi) = 100 \text{ MHz}$. To bring the upper two rows into tolerably good agreement with Alexei’s December 17, 2009 report at the BNL review, “After capture in barriers need to make ...”, I need to assume that the row labelled “Synchrotron tune” is actually “synchrotron frequency” which is 2π times the synchrotron tune. (Otherwise his $Q_s/(\Delta p/p)$ ratio seems impossibly high.)

Table 4: RF parameters assuming $G_{RF} = 2$, $\alpha_{\max-\max} = 0.5$ r, and $\omega_{RF}/(2\pi) = 100$ MHz.

$(\Delta p/p)_{\max.}$	$\Delta\gamma_{\max.}$	Q_s	$V_{RF}[\text{KV}]$	$t_{\max}[\text{ns}]$	$\ell_{\max}[\text{m}]$
0.0032	0.00143	0.01	172.6	0.796	0.143
0.0016	0.000715	0.00512	43.14	0.796	0.143
0.001	0.000447	0.00320	16.85	0.796	0.143
0.0008	0.000357	0.00256	10.79	0.796	0.143
0.00025	0.000112	0.00080	1.053	0.796	0.143
0.000075	0.0000335	0.00024	0.0948	0.795	0.143
0.000025	0.0000112	0.000080	0.0105	0.795	0.143

A APPENDICES

A.1 Excess Path Length Resulting from Betatron Oscillation

We study path length variation due to betatron oscillations. For a semi-quantitative numerical example we will use the equal-tune-FODO, circular lattice of radius ρ_0 described in Section 3. This model neglects both the geometric focusing in the bend field (which is usually small compared to separated function focusing) and the dependence of proton potential energy on radial position in a electrostatic lattice. The results will later be generalized to arbitrary lattices.

A.1.1 Horizontal Betatron Oscillations

We use cylindrical, $(\rho = \rho_0 + x, \phi = s/\rho_0, y)$ coordinates, where y replaces the vertical variable more conventionally denoted by z . In these coordinates, the path length ℓ of a particle orbit $\rho = \rho(\phi)$ lying in the horizontal plane is given by

$$\ell = \int_{\phi_1}^{\phi_2} d\phi \sqrt{\rho^2(\phi) + \left(\frac{d\rho}{d\phi}\right)^2} = \int_0^{\ell_0} ds \frac{\sqrt{\rho^2 + \rho_0^2 \rho'^2}}{\rho_0}, \quad (180)$$

where $\rho' \equiv d\rho/ds$ and ℓ_0 is the length of the design orbit. The orbit of a particle executing horizontal betatron oscillations with Courant-Snyder amplitude $\sqrt{\epsilon_x}$, is given by

$$\begin{aligned} \rho(s) &= \rho_0 + \sqrt{\epsilon_x \beta_x(s)} \cos(\psi_x(s) + \psi_{x,0}), \\ \rho'(s) &= \frac{1}{2} \sqrt{\frac{\epsilon_x}{\beta_x}} \beta'_x - \sqrt{\epsilon_x \beta_x(s)} \psi'_x \sin(\psi_x(s) + \psi_{x,0}) \\ &= \sqrt{\frac{\epsilon_x}{\beta_x}} \left(\frac{\beta'_x}{2} \cos(\psi_x(s) + \psi_{x,0}) - \sin(\psi_x(s) + \psi_{x,0}) \right), \end{aligned} \quad (181)$$

where $\psi_{x,0}$ is the initial betatron phase, $\psi_x(s)$ is the further phase advance through distance s , and $\psi'_x = 1/\beta_x$ has been used. Note that the first of Eqs. (181) serves to *define* the C-S invariant ϵ_x . As the phase $\psi_x(s)$ scans through all possible values, the maximum excursion at s is given by $\sqrt{\epsilon_x \beta_x(s)}$. Then

$$\rho^2 + \rho_0^2 \rho'^2 = \rho_0^2 \left(1 + \frac{2\sqrt{\epsilon_x \beta_x}}{\rho_0} \cos(\psi_x(s) + \psi_{x,0}) + \epsilon_x \frac{\mathcal{M}_1}{\rho_0^2} \right), \quad (182)$$

where

$$\mathcal{M}_1 = \beta_x \cos^2(\psi_x(s) + \psi_{x,0}) + \frac{\rho_0^2}{\beta_x} \left(\frac{\beta'_x}{2} \cos(\psi_x(s) + \psi_{x,0}) - \sin(\psi_x(s) + \psi_{x,0}) \right)^2. \quad (183)$$

The integrand of Eq. (180) can be expanded as

$$\frac{\sqrt{\rho^2 + \rho_0^2 \rho'^2}}{\rho_0} \approx 1 + \sqrt{\epsilon_x} \frac{\sqrt{\beta_x}}{\rho_0} \cos(\psi_x(s) + \psi_{x,0}) + \epsilon_x \mathcal{M}_2, \quad (184)$$

where

$$\begin{aligned} \mathcal{M}_2 &= \left(\frac{\mathcal{M}_1}{2\rho_0^2} - \frac{\beta_x \cos^2(\psi_x(s) + \psi_{x,0})}{2\rho_0^2} \right) \\ &= \frac{1}{2\beta_x} \left(\frac{\beta'_x}{2} \cos(\psi_x(s) + \psi_{x,0}) - \sin(\psi_x(s) + \psi_{x,0}) \right)^2. \end{aligned} \quad (185)$$

The orbit length is then

$$\ell \equiv \ell_0 + \Delta\ell_x = \int_0^{\ell_0} ds \left(1 + \sqrt{\epsilon_x} \frac{\sqrt{\beta_x(s)}}{\rho_0} \cos(\psi_x(s) + \psi_{x,0}) + \epsilon_x \mathcal{M}_2 \right). \quad (186)$$

The first term integrates to ℓ_0 , the length of the design orbit. To obtain the orbit length averaged over many turns one can average over $\psi_{x,0}$ since betatron phases are distributed uniformly. The second term vanishes in this averaging. Averaging the final term,

$$\langle \mathcal{M}_2(s) \rangle_{\psi_{x,0}} = \int_0^{2\pi} \frac{d\psi_{x,0}}{2\pi} \mathcal{M}_2(\psi_x(s), \psi_{x,0}) = \frac{1}{4\beta_x} \left(1 + \frac{\beta_x'^2}{2} \right) = \frac{\gamma_x}{4}, \quad (187)$$

where the other Twiss parameters, $\alpha_x = -\beta'_x/2$ and $\gamma = (1 + \alpha_x^2)/\beta_x$ have been used. Then the excess length is given by

$$\Delta\ell_x = \frac{\epsilon_x}{4} \int_0^{\ell_0} \gamma_x(s) ds. \quad (188)$$

This integral can be taken over the full ring or, equivalently, taken over individual elements and then summed. Note though that straight sections contribute to the path length excess.

Evaluating these integrals for the equal tune FODO lattice gives the dependence on machine tune Q_x of the averaged excess length coefficient shown in Fig. 8.

A.1.2 Vertical Betatron Oscillations

The path length in the presence of vertical betatron oscillations is given by a formula much like Eq. (180);

$$\ell = \int_{\phi_1}^{\phi_2} d\phi \sqrt{\rho^2(\phi) + \left(\frac{dy}{d\phi} \right)^2} = \int_0^{\ell_0} ds \frac{\sqrt{\rho^2 + \rho_0^2 y'^2}}{\rho_0}. \quad (189)$$

The equations governing vertical oscillations can be transcribed from Eq. (181), and the subsequent derivation proceeds as for horizontal oscillations. The final result, then, is

$$\Delta\ell_y = \frac{\epsilon_y}{4} \int_0^{\ell_0} \gamma_y(s) ds. \quad (190)$$

A.2 Relation Between Dispersion Function and the Closed Orbit Path Length Deviation Caused by a Local Deflection

Using sextupoles, one wishes to alter the closed orbit path length as a function of horizontal and/or vertical Courant-Snyder invariants. There is a remarkable formula relating path length deviation caused by a deflection $\theta_x|_P$ at lattice point P and the dispersion function $D|_P$ at the same point P. This appendix supplies a derivation of the result whose validity, seems to be well known[14], but whose derivation is hard to find documented.

The difference equation describing the perturbative effect of deflection θ_x occurring at a point (to be taken as the origin) on successive turns of horizontal betatron motion is

$$x_{j+1} - 2 \cos \mu_x x_j + x_{j-1} = \theta_x \beta_x(0) \sin \mu_x, \quad (191)$$

where $\mu_x = 2\pi Q_x$ is the once-around phase advance. (To derive this equation one applies the once-around transfer matrix (in Twiss form) to propagate the, deflected by $\theta_x/2$ orbit, forward by one turn and, with the inverse of the once-around transfer matrix, back-propagate the, undeflected by $\theta_x/2$ orbit, by one turn.) Solving this equation, one finds the closed orbit deviation and slope at the origin to be

$$\begin{aligned} x(0) &= \beta_x(0) \frac{\sin \mu_x}{2(1 - \cos \mu_x)} \theta_x = \beta_x(0) \frac{\cos(\mu_x/2)}{2 \sin(\mu_x/2)} \theta_x, \\ x'(0) &= -\alpha_x(0) \frac{\cos(\mu_x/2)}{2 \sin(\mu_x/2)} \theta_x. \end{aligned} \quad (192)$$

Propagating this result forward from the origin to longitudinal position s , one obtains

$$x(s) = \sqrt{\beta_x(0)\beta_x(s)} \frac{\cos(\psi_x - \mu_x/2)}{2 \sin(\mu_x/2)} \theta_x, \quad (193)$$

where ψ_x is the phase advance from the origin to s . (As well as satisfying the initial and final conditions at the origin, this function evolves correctly with s .)

We now use this result to derive two not-obviously-related quantities: the excess closed orbit path length $\Delta\ell$ resulting from the deflection θ_x ; and the dispersion function $D(0)$ at the origin. The excess path length $\Delta\ell = \ell - \ell_0$ is given by

$$\Delta\ell = \int_0^{\ell_0} \frac{x(s)}{\rho(s)} ds, = \theta_x \frac{\beta_x^{1/2}(0)}{2 \sin(\mu_x/2)} \int_0^{\ell_0} \frac{\beta_x^{1/2}(s)}{\rho(s)} \cos(\psi_x - \mu_x/2) ds. \quad (194)$$

On the other hand the dispersion function at the origin can be visualized as having resulted from the superposition of angular deflections $\delta(ds/\rho(s))$ due to the fractional rigidity offset δ through the ds intervals making up the ring;

$$D(0) = \delta \frac{\beta_x^{1/2}(0)}{2 \sin(\mu_x/2)} \int_0^{\ell_0} \frac{\beta_x^{1/2}(s)}{\rho(s)} \cos(\psi_x - \mu_x/2) ds. \quad (195)$$

Comparing these two equations yields the important result

$$\Delta\ell = D(0)\theta_x. \quad (196)$$

A.3 Sextupole Chromatic Neutrality

The purpose for the A and B sextupole families is to cancel path length dependence on horizontal and vertical betatron amplitudes. The purpose for the C sextupoles is to compensate for chromatic (i.e. γ -dependent) decoherence. At least part of this mission is to cancel any chromatic dependence on path length caused by the A and B sextupoles.

According to Eq. (155) dispersion-proportional displacement $D^A\delta$ at an A sextupole, causes an angular deflection $-(S^A/2)(D^A\delta)^2$, for fractional momentum offset δ . From Eq. (196) one sees that the resultant path length deviation is

$$\Delta\ell \approx -\frac{S^A D^{A3}}{2} (\gamma - \gamma_0)^2 \left(\frac{d\delta}{d\gamma}\right)^2. \quad (197)$$

The effect of A and B sextupoles can be counteracted by the C sextupoles by enforcing the condition

$$S^C D^{C3} = -S^A D^{A3} - S^B D^{B3}. \quad (198)$$

References

- [1] H. Kober, *Dictionary of Conformal Transformations*, Dover, p.22, 1957
- [2] G. Bennett, et al. *Electrostatic Focusing in the AGS g-2 Storage Ring*, p. 2070, PAC, 1993
- [3] A. Fedotov, *Beam Parameters and Collective Effects for pEDM Ring*, Dec. 7, 2009, BNL Review
- [4] A. Fedotov, pEDM_Beam_Parameters_Nov_2009.doc
- [5] S. Machida, *Space-Charge Effects in Circular Accelerators*, in *High Quality Beams*, AIP Conf. Proc. 592, S. Kurokawa et al., editors, p.405, 2000
- [6] W. Weng, *Space Charge Effects—Tune Shifts and Resonances*, in *Physics of Particle Accelerators*, AIP Conf. Proc. 153, M. Month and M. Dienes, editors, p.348, 1985
- [7] Proton EDM Storage Ring Collaboration, *R&D Development Plan for a Proton EDM Experiment with Sensitivity of 10^{-29} e.cm*, BNL Report Proton_RD_091125.pdf, 2009
- [8] H. Wollnik, *Optics of Charged Particles*, Academic Press, p. 124, 1987
- [9] J. Jackson, *Classical Electrodynamics*, 3rd edition, John Wiley, 1998
- [10] M. Sands, *The Physics of Electron Storage Rings— An introduction*, SLAC-121, 1970
- [11] D.V. Bugg, et al., *Proton-Proton Scattering at 970 MeV* Phys. Rev. **133**. B1017, 1964
- [12] F. Rathmann, et al., *Complete angular distribution measurements of pp spin correlation parameters A_{xx} , A_{yy} , and A_{xz} and analyzing power A_y at 197.4 MeV*, Phys. Rev. C, **58**, 658, 1998
- [13] <https://www.bnl.gov/edm/review/response/Response-polarimeter-techreview.pdf>
- [14] D. Rice, *Error Sources and Effects*, in *Handbook of Accelerator Physics and Engineering*, A. Chao and M. Tigner, editors, World Scientific, 2002